الجمهورية الجزائرية الديمقراطية الشعبية

People's Democratic Republic of Algeria
وزارة التعليم العالي و البحث العلمي
Ministry Of Higher Education And Scientific Research
جامعة الشهيد حمه لخضر الوادي
Echahid Hamma Lakhdar University Of El-Oued
كلية العلوم الطبيعة والحياة
Faculty Of Natural Sciences and Life
قسم البيولوجيا الخلوية والجزيئية
Department Of Cellular and Molecular Biology

THESIS

Submitted to obtain 2nd Cycle LMD Master degree

In Biological sciences

Specialty: Applied Biochemistry

THEME

Design, Characterization, and Efficacy of a Ferrocene-Derivative Dermal Cream Against Skin Inflammation and Redox Imbalance

Presented by:

AMARA Aya

BELAID Chiraz

DOUYEM Arfene Soundes

Discussed on:

Jury Members:

President	**Dr. HOUMRI Nawel**	**El-Oued University**
Supervisor	**Dr. Elhafnaoui LANEZ**	**El-Oued University**
Co-Supervisor	**Dr. Housseyn CHAOUA**	**El-Oued University**
Examiner	**Dr. MEHELLOU Zineb**	**El-Oued University**

University years : 2025/ 2026


بسم الله الرحمن الرحيم

DEDICATION

To my beloved parents, who have been my greatest blessing and the foundation of everything I am.

To my Mother, the heartbeat of my life, whose endless love, warmth, and prayers carried me through every difficult step of this journey.

To my Father, my source of pride and strength, who sacrificed so much to see me succeed, and whose belief in my capabilities never wavered.

Thank you both for giving me the wings to fly and the roots to stand strong.

To my dear brothers and my sweet sister, for being my safe haven and my constant source of joy. Thank you for your unconditional support, your laughter, and for always being by my side, making the heaviest days feel light.

And to myself, Amara Aya, with deep gratitude for the patience, the quiet resilience, and the strength to keep going when the path was long. This accomplishment is a beautiful reminder that every dream is within reach when you work with passion and dedication.

To the beautiful souls who made this dream possible, I lovingly dedicate this work.

✍ **Amara Aya**

إهداء

تحمل قلبي اليوم" عرفاناً "خالصاً، أهدي ثمرة هذا الجهد العلمي:

إلى أمي الغالية؛ رمز العطاء والدعم الصامت، من رافقتني بدعواتها الصادقة طيلة مشواري الدراسي وكان لوجودها الأثر الأكبر في ثباتي ونجاحي.

إلى أبي الغالي؛ سندي ومثلي الأعلى، يا من اخترتَ لي اسمي" عرفان "ليكبر معي، ها أنا اليوم أترجم اختيارك ليكون شكرًا حقيقيًا يليق بتضحياتك وسعيك الدائم لأجلي.

إلى إخوتي وأخواتي؛ السند الحقيقي والملاذ الآمن في كل الأوقات.

إلى أساتذي المشرف القدير، والأساتذة المساعدين في المختبر، وكافة الأساتذة الأفاضل الذين نهلتُ من علمهم، وإلى زميلاتي الشريكات في هذا العمل المتكامل.

أهديكم جميعاً حصاد تعبي وسهر سنواتي، تقديراً ووفاءً لنبل عطائكم.

سندس

الإهداء

الحمد لله الذي وفقني لإتمام هذا العمل المتواضع، والذي كان ثمرة تعب وصبر وسنوات من الاجتهاد، والصلاة والسلام على أشرف المرسلين سيدنا محمد صلى الله عليه وسلم.

أهدي هذا العمل إلى أعز ما أملك في هذه الحياة، إلى من كانت دعواتها سر نجاحي وقوتي، إلى أمي الغالية التي كانت سندي وراحتي في كل الأوقات، حفظها الله وأدامها نورًا في حياتي.

وإلى أبي العزيز، الذي علمني معنى الاجتهاد والصبر، وكان دائم الدعم والمساندة لي، أطال الله في عمره وبارك فيه.

وإلى أخواتي العزيزات :تقوى، نور، دعاء، وإكرام، اللواتي كنّ مصدر حب وتشجيع وسعادة، وشاركني لحظات التعب قبل الفرح.

كما أهدي هذا العمل إلى كل شخص وقف بجانبي، وساندني نفسيًا ومعنويًا، ولو بكلمة طيبة أو دعوة صادقة، وإلى كل من آمن بقدراتي وشجعني على مواصلة الطريق.

وإلى نفسي، التي صبرت واجتهدت ولم تستسلم رغم كل الصعوبات.

وفي الأخير، أسأل الله أن تجعل هذا العمل نافعًا ومباركًا.

بالعيد شراز

Acknowledgment

We would like to extend our deepest gratitude, utmost respect, and sincere appreciation to our esteemed supervisor, Professor Elhafnaoui Lanez.

Words seem insufficient to express how grateful we are for his invaluable scientific guidance, his immense patience, and his unwavering support throughout the development of this thesis. From the very beginning, Professor Lanez has been a beacon of knowledge and a source of profound inspiration. His insightful critiques, rigorous scientific standards, and brilliant remarks have not only shaped the structure of this academic work but have also fundamentally elevated our understanding of research.

Beyond his exceptional academic mentorship, we are profoundly grateful for his kindness, his continuous encouragement during moments of doubt, and his dedication to bringing out the best in his students. He did not merely supervise a thesis; he nurtured researchers.

We consider it a great privilege and a true honor to have conducted this research under his wise and distinguished supervision. The academic and personal lessons we have learned from him are invaluable assets that we will carry proudly into our future careers. Thank you, Professor, for your time, your generosity, and for being an exemplary role model of scientific excellence.

.

ABSTRACT

This study evaluates the therapeutic efficacy of three functionalized organometallic formulations based on synthesized ferrocene derivatives (FMA, FCMphA, and FCMphB) as topical treatments for severe thermal burns. Severe burns trigger localized necrosis, marked cutaneous lipid peroxidation, and a Systemic Inflammatory Response Syndrome (SIRS) that severely impacts immune organs. Through a comparative analysis, we performed specific in vivo biochemical, hematological, and histopathological assays on Wistar rats, using the standard drug MEBO as a reference control.

Our practical findings demonstrated that the tested ferrocene ointments significantly accelerated healing mechanics. FMA emerged as the most efficient formulation, dramatically reducing the epithelialization time to 17±5 days (compared to 29 days in untreated controls and 33 days for MEBO). At the systemic level, treatment with these derivatives induced a near-complete normalization of the burn-induced leukocyte profile (WBC, LYM, and GRA) and effectively reversed reactive thrombocytosis. Furthermore, these formulations successfully mitigated immune organ dysregulation, restoring the burn-induced splenic hypertrophy and thymic involution back to normal physiological ranges while establishing an excellent safety profile free of hepatic or renal toxicities.

Biochemically, the topical application of these compounds completely suppressed cutaneous lipid peroxidation by reducing malondialdehyde (MDA) levels and significantly restoring endogenous antioxidant defenses (GSH, SOD, and CAT) at the injury site. To elucidate these findings, an in silico molecular docking study was carried out against two regulatory protein targets: KEAP1 and MMP-9. The computational results corroborated the experimental evidence, revealing that FMA and FCMphB possess exceptional binding free energies, driving a dual mechanism of action that couples Nrf2-mediated antioxidant defense with controlled extracellular matrix remodeling. Collectively, this integrated work positions functionalized ferrocene derivatives as highly biocompatible, multi-targeted candidates for advanced burn wound therapeutics.

Keywords: Applied Biochemistry, Ferrocene Derivatives (FMA, FCMphA, FCMphB), In Vivo Burn Model, Burn-Induced Inflammation, Cutaneous Oxidative Stress, Immunomodulation, Molecular Docking (KEAP1/MMP-9), Rates**.**

RÉSUMÉ

Cette étude évalue l'efficacité thérapeutique de trois formulations organométalliques fonctionnalisées basées sur des dérivés de ferrocène synthétisés (FMA, FCMphA et FCMphB) en tant que traitements topiques pour les brûlures thermiques graves. Les brûlures graves déclenchent une nécrose localisée, une peroxydation lipidique cutanée marquée et un Syndrome de Réponse Inflammatoire Systémique (SIRS) qui affecte gravement les organes immunitaires. À travers une analyse comparative, nous avons réalisé des essais biochimiques, hématologiques et histopathologiques in vivo spécifiques sur des rats Wistar, en utilisant le médicament standard MEBO comme témoin de référence.

Nos résultats pratiques ont démontré que les pommades de ferrocène testées accéléraient de manière significative les mécanismes de cicatrisation. Le FMA s'est révélé être la formulation la plus efficace, réduisant considérablement le temps d'épithélialisation à 17±5 jours (contre 29 jours pour les témoins non traités et 33 jours pour le MEBO). Au niveau systémique, le traitement avec ces dérivés a induit une normalisation quasi-complète du profil leucocytaire induit par la brûlure (WBC, LYM et GRA) et a inversé efficacement la thrombocytose réactive. De plus, ces formulations ont atténué avec succès le dysfonctionnement des organes immunitaires, rétablissant l'hypertrophie splénique et l'involution thymique induites par la brûlure vers des plages physiologiques normales, tout en établissant un excellent profil de sécurité exempt de toxicités hépatiques ou récentes.

Sur le plan biochimique, l'application topique de ces composés a complètement supprimé la peroxydation lipidique cutanée en réduisant les taux de malondialdéhyde (MDA) et en restaurant de manière significative les défenses antioxydantes endogènes (GSH, SOD et CAT) au niveau du site de la blessure. Pour élucider ces résultats, une étude de docking moléculaire in silico a été réalisée contre deux cibles protéiques régulatrices : KEAP1 et MMP-9. Les résultats informatiques ont corrigé et corroboré les preuves expérimentales, révélant que le FMA et le FCMphB possèdent des énergies libres de liaison exceptionnelles, entraînant un double mécanisme d'action qui couple la défense antioxydante médiée par Nrf2 avec le remodelage contrôlé de la matrice extracellulaire. Collectivement, ce travail intégré positionne les dérivés de ferrocène fonctionnalisés comme des candidats multi-cibles hautement biocompatibles pour la thérapeutique avancée des brûlures.

Mots-clés : Biochimie Appliquée, Dérivés de Ferrocène (FMA, FCMphA, FCMphB), Modèle de Brûlure In Vivo, Inflammation Induite par les Brûlures, Stress Oxydatif Cutané, Immunomodulation, Docking Moléculaire (KEAP1/MMP-9)**,** Rates.

ملخص

تُقيّم هذه الدراسة الفعالية العلاجية لثلاث تركيبات عضويّة معدنيّة (Organometallic Formulations) وظيفية تعتمد على مشتقات الفيروسين المصنعة وهي FMA) و FCMphA و (FCMphB كعلاجات موضعية للحروق الحرارية الشديدة .تتسبب الحروق الشديدة في حدوث نخر موضعي (Localized necrosis)، وبيروكسيد الدهون الجلدي(Cutaneous lipid peroxidation) ، ومتلازمة الاستجابة الالتهابية الجهازية (SIRS) التي تؤثر بشدة على الأعضاء المناعية .ومن خلال تحليل مقارن، أجرينا تحاليل مخبرية بيوكيميائية، وهيماتولوجية، وهستوباثولوجية نوعية في الجسم الحي (In vivo) على جرذان من سلالة ويسر(Wistar rats) ، باستخدام الدواء القياسي ميبو (MEBO) كمرجع للمقارنة.

أظهرت نتائجنا التطبيقية أن مراهم الفيروسين المختبرة سرعت بشكل ملحوظ من آليات الشفاء .وبرز مركب FMA كأكثر التركيبات كفاءة، حيث قلل بشكل كبير من وقت تشكل النسيج الطلائي (Epithelialization time)إلى 5±17 يوماً) مقارنة بـ 29 يوماً في مجموعات المراقبة غير المعالجة و 33يوماً لـ .(MEBO على المستوى الجهازي، أدى العلاج بهذه المشتقات إلى عودة شبه كاملة للمؤشرات اللوكوسيتية لخلايا الدم البيضاء WBC) و LYM و (GRA المعدلة بالحرق إلى طبيعتها، كما عكس بفعالية كثرة الصفيحات التفاعلي .(Reactive thrombocytosis) علاوة على ذلك، نجحت هذه التركيبات في التخفيف من خلل تنظيم الأعضاء المناعية، حيث أعادت تضخم الطحال (Splenic hypertrophy)والضمور الزعتري (Thymic involution) الناجم عن الحروق إلى النطاقات الفسيولوجية الطبيعية، مع إثبات ملف أمان ممتاز خالٍ من أي سمية كبدية أو كلوية.

من الناحية البيوكيميائية، أدى التطبيق الموضعي لهذه المركبات إلى تثبيط كامل لبيروكسيد الدهون الجلدي عن طريق خفض مستويات المالونديالدهيد (MDA) واستعادة الدفاعات المضادة للأكسدة الداخلية بشكل ملحوظ GSH) و SOD و (CAT في موقع الإصابة .ولتوضيح هذه النتائج، أُجريت دراسة نمذجة جزيئية حاسوبية (In silico molecular docking) ضد هدفين من البروتينات التنظيمية وهما KEAP1 :و MMP-9.وجاءت النتائج الحاسوبية متوافقة مع الأدلة التجريبية، حيث كشفت أن مركبي FMA و FCMphBيمتلكان طاقات ارتباط حرة استثنائية(Binding free energies) ، مما يفعّل آلية عمل مزدوجة تربط بين الدفاع المضاد للأكسدة بوساطة Nrf2 وتنظيم تفكيك المصفوفة خارج الخلوية (Extracellular matrix remodeling).ختاماً، يضع هذا العمل المتكامل مشتقات الفيروسين الوظيفية كمرشحات ممتازة متعددة الأهداف وموافقة حيوياً (Biocompatible) لعلاجات الحروق المتقدمة.

الكلمات المفتاحية :الكيمياء الحيوية التطبيقية(Applied Biochemistry) ، مشتقات الفيروسين (Ferrocene Derivatives)، نموذج الحرق في الجسم الحي(In Vivo Burn Model) ، التهابات الحروق(Burn-Induced Inflammation) ، الإجهاد التأكسدي الجلدي (Cutaneous Oxidative Stress)، التعديل المناعي(Immunomodulation) ، النمذجة الجزيئية (Molecular Docking KEAP1/MMP-9)، فئران.

Table of content

Content

Liste of figures

Liste of Tables

INTRODUCTION

Introduction

In the field of modern applied biochemistry, evaluating the interaction between therapeutic macromolecules and cellular systems is essential for developing novel clinical treatments. Severe cutaneous injuries, such as third-degree thermal burns, induce complex biochemical alterations that rapidly extend from local tissues into systemic physiological pathways (Jeschke et *al.*, 2008). At the cellular level, thermal trauma triggers biochemical cascades that alter blood parameter kinetics and induce reactive structural changes in primary immune organs (Choromanska et *al.*, 2012). Concurrently, the central process driving this post-burn pathogenesis is the severe propagation of oxidative stress, where the accumulation of free radicals damages biological membranes, leading to lipid peroxidation and increasing systemic tissue inflammation (Ayala et *al.*, 2014; Bladh et *al.*, 2020).

To control these destructive biomolecular pathways, applied biochemistry utilizes targeted bioactive complexes designed to safely interact with damaged biological environments. Functionalized metallocene compounds, particularly ferrocene derivatives, have emerged as highly efficient biomaterials due to their chemical stability and enhanced lipophilicity, which allows them to cross biological lipid bilayers (Biot et *al.*, 2004). Most importantly, their reversible electron-transfer kinetics enable these molecules to operate as efficient biochemical buffers capable of scavenging free radicals and protecting critical biomolecules from oxidative degradation (Ornelas, 2012).

Therefore, the objective of this work is to bridge the gap between biochemical mechanisms and burn pathology. To achieve this, the dissertation is structured into four main chapters. Chapter I establishes the theoretical and biochemical framework regarding ferrocene compounds. Chapter II details the pathophysiology of burn-induced inflammation and oxidative stress. Chapter III comprehensively outlines the Materials and Methods utilized in both the experimental bioassays and the computational modeling. Finally, Chapter IV is dedicated to the comprehensive Results and Discussion, integrating both the in vivo and in silico outcomes. Ultimately, this integrated work opens scientific pathways for utilizing functionalized derivatives as biocompatible antioxidant tools in advanced tissue healing.

FIRST PART

Bibliographic synthesis

CHAPTER I

Overview of Ferrocene

I.1. Overview of Ferrocene

I.1.1. Discovery and Structural Architecture

The historical landscape of coordination and organometallic chemistry experienced a monumental paradigm shift in the winter of 1951. This transformation occurred when Thomas J. Kealy and Peter L. Pauson accidentally isolated an unprecedented, highly stable orange crystalline compound during their laboratory attempts to synthesize fulvalene using iron(III) chloride and cyclopentadienylmagnesium bromide (Kealy & Pauson, 1951). Concurrently and via a completely independent synthetic pathway, Samuel A. Miller, John A. Tebboth, and John F. Tremaine synthesized and reported the exact same organo-iron substance by reacting volatile cyclopentadiene directly with reduced iron at elevated temperatures (Miller et *al.*, 1952). At the time of its accidental synthesis, the structural arrangement proposed did not account for the molecule's extraordinary chemical resilience.

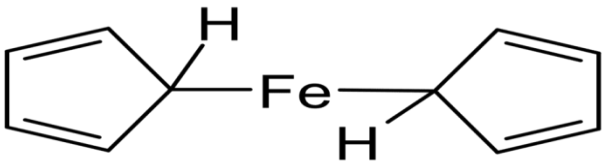

Figure I-1: *Initial non-sandwich structure of ferrocene proposed by Kealy and Pauson (1951).*

The architectural mystery was officially resolved in 1952, when the eminent scientists Ernst Otto Fischer and Geoffrey Wilkinson independently deduced its revolutionary, non-classical geometric configuration. They demonstrated that the molecule possesses a unique symmetric "sandwich" morphology, a groundbreaking discovery that fundamentally altered the established theories of chemical bonding and subsequently earned both researchers the Nobel Prize in Chemistry in 1973 (Fischer & Pfab, 1952; Wilkinson et *al.*, 1952).

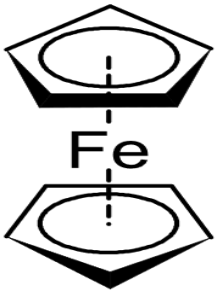

Figure I-2: *Modern 3D molecular sandwich structure of ferrocene as determined by Fischer and Wilkinson.*

From a crystallographic perspective, ferrocene ([Fe(C5H5)2], frequently abbreviated as [Fe(Cp)2]) is classified as the quintessential archetype of the metallocene family. The structural framework of this organometallic complex consists of a central transition metal iron atom, maintaining a +2 oxidation state (Fe2+), which is structurally sandwiched and symmetrically coordinated between two parallel, planar, and aromatic cyclopentadienyl (Cp-, C5H5-) rings (Wilkinson, 1974). Within this conformation, the bonding matrix does not manifest as a localized sigma-bond between the iron center and a specific carbon atom. Rather, it is characterized by an extensive, delocalized haptic (η5) overlap, wherein the d-orbitals of the central Fe2+ cation share electron density equally with the combined ten carbon atoms of both overlapping π-electron clouds (Elschenbroich, 2006).

This unique chemical bonding architecture allows the cyclopentadienyl rings to rotate around the vertical symmetry axis with an exceptionally low energy barrier, fluctuating systematically through a series of conformational rotations. As illustrated in conformational potential energy maps, the molecule continuously shifts between the eclipsed state (D5h) and the staggered state (D5d) (Elschenbroich, 2006). Specifically, during a full rotational trajectory, intermediate geometries present structural variations at specific angular coordinates; rotations at 18°, 72°, and 90° systematically align the carbon frameworks toward the eclipsed state, whereas dynamic progression through conformational configurations at 36°, 54°, and 108° drives the rings into the thermodynamically distinctive staggered isomerism. This fluid conformational flexibility confirms that the robust organometallic core can serve as a highly adaptable macromolecular template for subsequent strategic functionalizations.

I.1.2. Chemical Synthesis and Laboratory Preparation

The development of reproducible and highly efficient synthetic pathways for the production of pristine ferrocene represents a critical milestone in organometallic engineering. These methods facilitated the transition from its historical accidental isolation to extensive industrial exploitation and contemporary medicinal applications. Synthesizing this bis(η5-cyclopentadienyl)iron(II) core essentially relies on the strategic deprotonation of cyclopentadiene (C5H6) monomer precursors followed by stoichiometric coordination with a suitable iron(II) source. In rigorous laboratory settings, two primary and peer-reviewed synthetic methodologies are widely recognized:

- **The Classical Grignard Pathway:** This traditional mechanism involves the initial generation of cyclopentadienylmagnesium bromide via the reaction of freshly cracked, monomeric cyclopentadiene with an organic Grignard reagent in anhydrous diethyl ether or

tetrahydrofuran (THF). Subsequent addition of anhydrous iron(II) chloride ($FeCl_2$) under a strict inert gas atmosphere induces rapid transmetalation and coordination, precipitating high-purity, orange crystalline ferrocene flakes (Wilkinson et *al.*, 1952).

- **The Amine-Mediated Base Pathway:** To improve experimental yields and minimize the hazardous constraints of Grignard handling, contemporary protocols prioritize the use of powerful organic amine bases, such as diethylamine or dimethyl sulfoxide (DMSO)-potassium hydroxide systems. The organic base efficiently abstracts the relatively acidic methylene proton from volatile cyclopentadiene, instantly generating the stable nucleophilic cyclopentadienyl anion (Cp^-). These generated anions rapidly encapsulate solvated Fe^{2+} cations, establishing the highly stable, symmetric thermodynamic sandwich core with exceptional reaction efficiency (Jolly, 1970).

These established preparation techniques yield a pure, non-reactive solid crystal. In contemporary drug-design setups, this pristine core serves as a clean substrate for subsequent electrophilic aromatic substitution (EAS) protocols—such as Friedel-Crafts acylation or alkylation—which enable researchers to custom-decorate the cyclopentadienyl rings with targeted bioactive side-chains (Woodward et *al.*, 1952). To optimize these classical synthetic pathways for biomedical integration, modern approaches rely on validated reviews that synthesize structural variations and yield optimizations under controlled reaction conditions (Chao et *al.*, 2026).

I.1.3. Main Physicochemical Properties

In the domain of advanced drug design and macromolecular pharmacology, pristine ferrocene exhibits an extraordinary combination of physical and chemical characteristics that distinguish it from purely organic aromatic compounds:

- **Thermodynamic Resilience and the 18-Electron Rule:** The primary factor responsible for the profound chemical stability of ferrocene is its strict adherence to the 18-electron rule, achieving a closed-shell electronic configuration analogous to noble gases (Astruc, 2000). The central Fe^{2+} ionic core provides 6 valence d-electrons, while each of the two stabilizing aromatic Cp^- rings contributes 6 delocalized π-electrons, culminating in an optimal 18-electron valence shell. Consequently, this electronic configuration provides the molecule with extreme thermal stability, allowing it to withstand temperatures up to 400°C, while remaining highly resistant to degradation by concentrated alkaline solutions or strong, non-oxidizing acids.

- **Lipophilic Character and Cutaneous Bioavailability:** Ferrocene is intensely hydrophobic, entirely insoluble in aqueous environments, but demonstrates exceptional Public solubility in non-polar organic solvents. It possesses a highly favorable lipophilic partition coefficient (log P ≈ 2.7 to 3.5). In clinical dermatology and topical pharmacology, this pronounced lipophilicity serves as a vital biochemical asset; it provides ferrocene-containing ointments with the capacity to effectively cross compromised lipid bilayers and cellular membranes, ensuring deep, uniform therapeutic penetration into the ischemic and necrotic layers of deep burn injuries (Ornelas, 2011).
- **Volatility via Sublimation:** A distinct physical characteristic of ferrocene is its capacity to undergo direct sublimation at moderate temperatures, transforming from a solid crystal directly into a gas phase, a property heavily utilized in laboratory protocols for high-purity isolation.
- **Core Bioisosterism and Absolute Biocompatibility:** In medicinal chemistry, the three-dimensional, aromatic ferrocene nucleus is recognized as an ideal bioisostere for classical, flat phenyl rings. Crucially, despite containing a transition heavy metal, the powerful covalent-like iron-π coordination safely encapsulates the iron within the carbon cages. This prevents the premature or spontaneous intracellular release of free iron ions, which would otherwise trigger toxic Fenton reactions (Biot et *al.*, 2004). This structural safety profile guarantees low intrinsic cytotoxicity and outstanding systemic biocompatibility.

I.1.4. Redox Activity

The foundational engine that drives the biological, antioxidant, and tissue-remodeling capabilities of ferrocene-based therapies is its one-electron, highly reversible oxidation-reduction (Redox) behavior. Under mild physiological, electrochemical, or metabolic conditions, the chemical formulation of physical neutral, reduced ferrocene (Fe2+, lipophilic) can readily undergo a clean, single-electron loss to transition into the highly stable, water-soluble ferricenium radical cation (Fe3+, hydrophilic) (Conover & Toscano, 2015):

Ferrocene (Fe2+) ⇌ Ferricenium (Fe3+) + e-

This rapid and completely reversible electrochemical kinetics allows the metallocene complex to operate as a highly dynamic, localized "electronic sponge" within compromised biological matrices. Crucially, the exact oxidation potential required to trigger this reversible electron transfer is not rigid; it can be precisely tuned, shifted, or adapted by altering the inductive or resonance chemical effects of the functional groups substituted onto the cyclopentadienyl rings (Gasser et *al.*, 2011). Consequently, when applied topically to cutaneous

environments devastated by thermal trauma—where mass cellular lysis and localized hypoxia generate lethal cascades of Reactive Oxygen Species (ROS)—this continuous redox cycling allows the metallocene core to systematically scavenge destructive free radicals and interrupt the propagation pathways of lipid peroxidation (Hillard et *al.*, 2010).

I.2. Biological Activities of Ferrocene Derivatives

Ferrocene and its derivatives have emerged as highly attractive scaffolds in medicinal chemistry due to their remarkable sandwich-like organometallic structure, high chemical stability, low inherent toxicity, and reversible redox properties (Kedadra, 2022). The lipophilic character of the metallocene core, combined with the versatility of functionalizing its cyclopentadienyl (Cp) rings, allows these compounds to easily cross biological membranes and interact with diverse macromolecular targets. This unique interplay between coordination chemistry and clinical pharmacology endows ferrocene-based compounds with a wide range of biological activities, making them promising therapeutic candidates for tissue repair, wound healing, and burn management.

I.2.1. Antioxidant Activity

The antioxidant efficiency of ferrocene derivatives is inherently governed by the reversible, single-electron redox cycling of the central iron core between the ferrous (Fe2+) and ferric (Fe3+) oxidation states (Fouda et *al.*, 2007). In severe thermal injuries, the disruption of local cutaneous blood flow triggers an overwhelming and pathological accumulation of Reactive Oxygen Species (ROS), such as superoxide (O2•−) and hydroxyl (OH•) radicals. This localized oxidative stress induces extensive lipid peroxidation of cellular membranes, expanding the zone of necrosis and severely delaying the onset of the proliferative phase of healing.

The fundamental mechanism underlying this protective activity relies on the metallocene center acting as an electron donor to quench unstable radicals, transitioning through a stable ferrocenium cation intermediate, as represented in the following redox equilibria:

$$Cp2Fe \rightleftharpoons Cp2Fe+ + e-$$

$$Cp2Fe + OH\bullet + H+ \rightarrow Cp2Fe+ + H2O$$

Electrochemical and theoretical investigations carried out at the University of El-Oued demonstrate that N-ferrocenylmethylamines act as potent radical scavengers, where the chemical configuration and the nature of substituents on the aromatic ring significantly

influence the oxidation potential (Epa) of the ferrocene moiety (Kedadra, 2022; Lanez et *al.*, 2019). These organometallic complexes effectively neutralize free radicals through electron or hydrogen atom transfer mechanisms. The stability of the resulting interactions is further enhanced by long-range electrostatic forces, hydrophobic effects, and hydrogen bonding within the microenvironment (Kedadra, 2022).

By trapping free radicals at the injury site, topical application of these derivatives significantly suppresses lipid peroxidation, which is clinically manifested by a profound, dose-dependent decrease in malondialdehyde (MDA) levels in the treated tissues. Simultaneously, these compounds protect and upregulate the endogenous enzymatic antioxidant defense system, restoring the optimal physiological activities of superoxide dismutase (SOD), catalase (CAT), and reduced glutathione (GSH). Furthermore, advanced in silico molecular docking simulations reveal that these functionalized derivatives exhibit exceptional binding affinities and structural stability when docked into the pocket of the KEAP1 protein. This molecular target serves as the primary negative regulator of the Nrf2 pathway; thus, its inhibition by ferrocene compounds facilitates the nuclear translocation of Nrf2, promoting the transcriptional upregulation of cytoprotective and antioxidant genes necessary to counteract burn-induced oxidative trauma.

I.2.2. Anti-inflammatory Activity

Thermal destruction of the skin barrier initiates a robust and immediate inflammatory cascade. Although a transient inflammatory phase is crucial for clearing cellular debris and preventing immediate systemic infection, prolonged or hyperactive immune cell infiltration triggers a state of chronic inflammation. This chronic state perpetuates tissue degradation and stalls essential re-epithelialization. Ferrocene derivatives exert profound anti-inflammatory control by modulating both systemic hematological parameters and localized enzymatic cascades.

Systemically, severe burns frequently induce Systemic Inflammatory Response Syndrome (SIRS), characterized by a pathological escalation in circulating white blood cells (WBCs), granulocytes, lymphocytes, and blood platelets (thrombocytes), alongside a reactive hypertrophy of primary immune organs (Marck et *al.*, 2013). Treatment with optimized ferrocene ointments achieves a comprehensive resolution of this systemic response. It successfully normalizes elevated leukocyte and platelet counts and restores the physiological weight indices of the spleen and thymus back to healthy baselines. This confirms that these organometallic complexes limit the over-activation of the immune system without causing systemic immunosuppression or organ toxicity.

At the molecular level, in silico docking profiles demonstrate that N-ferrocenylmethylamine derivatives fit precisely into the active binding site of Matrix Metalloproteinase-9 (MMP-9), establishing low binding energies and a web of stable hydrophobic and hydrogen bonds. MMP-9 is an enzyme overexpressed during chronic inflammation that degrades the extracellular matrix (ECM) and delays mechanical wound closure. By effectively inhibiting MMP-9 activity, ferrocene formulations truncate the inflammatory phase and accelerate the transition into the proliferative phase. This enzymatic regulation facilitates the structured synthesis, deposition, and alignment of thick collagen bundles within the newly forming dermis, reducing scar formation and enhancing the tensile strength of the regenerated tissue.

I.2.3. Antimicrobial Activity

The necrotic, protein-rich environment of an open third-degree burn wound provides an ideal substrate for opportunistic microbial colonization by pathogenic strains such as Staphylococcus aureus and Pseudomonas aeruginosa. If left unchecked, microbial bio-burden halts wound contraction, degrades structural proteins, and risks progressing into fatal systemic sepsis. Traditional purely organic antibiotics face rising challenges due to microbial resistance pathways; in contrast, organometallic systems offer a distinct advantage via multi-targeted mechanisms of action.

The antimicrobial prowess of ferrocene derivatives is highly dependent on their lipophilic character, typically quantified by their calculated octanol/water partition coefficients (log P) (Kedadra, 2022). Functionalized N-ferrocenylmethylamines possess optimal lipophilicity, allowing them to effectively partition into and traverse the hydrophobic lipid bilayers of microbial cell membranes. Once inside the pathogen, the metallocene core participates in intracellular redox cycling, generating a highly localized burst of lethal ROS. These radicals induce non-specific oxidative damage to critical bacterial biomolecules, including DNA strands, metabolic enzymes, and membrane lipids, leading to cellular lysis.

Crucially, computational drug-likeness screening confirms that these specific ferrocene derivatives adhere strictly to Lipinski’s rule of five and Veber’s parameters, indicating high topical bioavailability, favorable membrane permeability, and low molecular flexibility. This allows the active ointments to efficiently penetrate through thick burn eschars and reach the deep dermal layers. By maintaining a sterile or low-bioburden wound bed, these derivatives dramatically accelerate the kinetics of wound healing, which is evidenced by rapid eschar

detachment, a shortened epithelialization period, and a near-complete morphological restoration of a continuous, functional epidermis.

I.3. Ferrocene in Wound Healing

1.3.1. ROS Modulation

The elevated production of reactive oxygen species (ROS) in wounded sites triggers several harmful effects, including cellular senescence, fibrotic scar formation, and inflammation. Therefore, reducing oxidative stress in the wound microenvironment may promote regenerative wound healing. ROS-scavenging nanocapsules are considered effective in wound treatment because of their antioxidative activity and targeted therapeutic effects. In this context, a highly versatile ferrocene-functionalized polymer was synthesized through one-pot radical polymerization to formulate self-assembled ferrocene nanocapsules (FNCs). These nanocapsules served as smart carriers for the antioxidant α-tocopherol (TP), demonstrating high stability and loading efficiency. The TP-loaded FNCs exhibited ROS-sensitive properties and significantly improved antioxidant activity compared to unloaded TP. Moreover, they reduced oxidative damage in mouse NIH 3T3 fibroblasts and promoted infected wound healing, confirming their potential as an ROS-mediated drug delivery system for oxidative stress-associated diseases (Na *et al.*, 2021).

CHAPTER II

Inflammation

II.1. Inflammation and Tissue Injury

II.1.1. General Concept of Inflammation

From a pathophysiological perspective, inflammation represents a fundamental, evolutionary conserved homeostatic response of vascularized tissues directed against cellular injury, pathogenic invasion, or severe physical and thermal disruption (Kumar *et al.,* 2020). Within the research context of functionalized biomolecules at the University of El-Oued, inflammation is evaluated not merely as a localized symptom, but as a complex biochemical cascade essential for initiating tissue regeneration (Kedadra, 2022). The ultimate biological goal of this process is defensive: to isolate and neutralize the primary etiological agent, clear out the resulting necrotic debris via phagocytosis, and orchestrate the cellular microenvironment required for structural remodeling (Snyder *et al.,* 2016). However, in cases of severe trauma such as high-degree thermal burns, the intense and persistent activation of this cascade can override physiological control, converting a protective mechanism into a secondary destructive process that induces microvascular damage and delays clinical healing (Punchard *et al.,* 2004).

II.1.1.1. Definition and Classification (Acute vs. Chronic)

In accordance with standard toxicological and pathological criteria, the inflammatory response is systematically classified into two distinct, yet interconnected phases based on the kinetics of cellular infiltration, onset velocity, and chronological duration (Kumar *et al.,* 2020):

• Acute Inflammation: This phase constitutes the immediate, non-specific early response to tissue insult, initiating within minutes to hours post-injury. Pathophysiologically, it is driven by rapid hemodynamic alterations, including transient arteriolar vasoconstriction followed by sustained vasodilation and increased microvascular permeability. These changes facilitate the active exudation of plasma proteins and fluid into the interstitial spaces, establishing localized edema (Kumar *et al.,* 2020). Mechanistically, the acute phase is cellularly defined by the selective and massive transmigration of polymorphonuclear leukocytes (PMNs)—predominantly neutrophils—which are guided by chemotactic gradients to the epicentre of injury (Snyder *et al.,* 2016).

• Chronic Inflammation: When the initial injury is sustained, or when localized biochemical signals fail to achieve timely resolution, the tissue transitions into chronic inflammation. This prolonged pathological state, extending from weeks to several months, involves a fundamental shift in the cellular landscape. The short-lived neutrophilic population is replaced by an influx of mononuclear leucocytes, specifically active macrophages, T and B lymphocytes, and plasma cells (Punchard *et al.,* 2004). Chronic inflammation is highly

detrimental to cutaneous architecture because it involves a simultaneous, destructive cycle of active tissue necrosis, prolonged immunological stress, and disorganized, frustrated attempts at fibrotic repair and angiogenesis (Kumar *et al.*, 2020).

II.1.1.2. The Five Cardinal Signs of Inflammation

At the clinical and morphological level, the localized manifestations of acute inflammation are governed by five classic hallmark criteria. These phenotypic changes are direct physiological consequences of the microvascular adaptations and neurological signaling cascades triggered within the damaged dermal layers (Punchard *et al.*, 2004; Kumar *et al.*, 2020):

1. Rubor (Redness): Induced by the localized relaxation of vascular smooth muscle, resulting in active vasodilation and an increased volumetric flow of blood (hyperemia) through the local capillary beds.

2. Tumor (Swelling): Developed as a consequence of endothelial cell contraction, which elevates microvascular permeability and allows the escape of macromolecular plasma proteins into the extravascular compartment, driving fluid accumulation and localized edema.

3. Calor (Heat): Resulting from the increased perfusion of core-temperature arterial blood to the peripheral injury site, coupled with the metabolic energy dissipated by hyperactive inflammatory cells during phagocytosis.

4. Dolor (Pain): Triggered biochemically by the accumulation of nociceptive chemical mediators (such as bradykinin, prostaglandins, and histamine) that lower the threshold of local nerve endings, aggravated mechanically by the physical pressure of edematous swelling.

5. Functio Laesa (Loss of Function): Representing the cumulative structural and neurological consequence of the injury, where normal physiological movement or cellular operation of the affected cutaneous area is temporarily or permanently impaired due to pain reflexes and tissue disorganization.

II.1.1.3. Inflammation as a Regulatory Bridge in Wound Healing Phases

Within the physiological framework of cutaneous tissue engineering, the inflammatory phase does not operate as an isolated pathological event; instead, it serves as a critical regulatory bridge linking initial vascular trauma to definitive structural closure. Cutaneous repair progresses through four highly regulated, overlapping temporal phases: hemostasis, inflammation, proliferation, and tissue remodeling (Wallace *et al.*, 2026).

The molecular signaling network established during the inflammatory phase dictates the kinetic success of the subsequent proliferative phase (Snyder *et al.,* 2016). Specifically, active macrophages embedded within the wound bed act as master regulators by executing a vital phenotypic switch from a pro-inflammatory, cytotoxic M1 phenotype to an anti-inflammatory, pro-healing M2 phenotype. This functional transition triggers the secretion of essential growth factors that stimulate dermal fibroblasts to migrate and synthesize a new extracellular matrix (fibroplasia), induce endothelial cells to sprout functional capillaries (Angiogenesis), and stimulate marginal keratinocytes to proliferate across the wound bed (re-epithelialization) (Wallace *et al.*, 2026). If this regulatory bridge is disrupted—as characteristically observed in deep thermal burns where the M1-to-M2 switch is delayed—the wound microenvironment becomes arrested in a chronic hyper-inflammatory loop, leading to progressive tissue autodigestion and pathological fibrosis.

II.1.2. Cellular and Molecular Mediators of Inflammation

II.1.2.1. Inflammatory Cell Influx (Neutrophils and Macrophages M1/M2)

In an inflammatory setting, macrophages can be polarized to an inflammatory M1 phenotype or to an anti-inflammatory M2 phenotype, as well as existing on a spectrum between these two extremes. Dysfunction of this phenotypic switch can result in a population imbalance that leads to chronic wounds or disease due to unresolved inflammation. Therapeutic interventions that target macrophages have therefore been proposed and implemented in diseases that feature chronic inflammation such as diabetes mellitus and atherosclerosis. We have developed a model for the sequential influx of immune cells in the peritoneal cavity in response to a bacterial stimulus that includes macrophage polarization, with the simplifying assumption that macrophages can be classified as M1 or M2. With this model, we were able to reproduce the expected timing of sequential influx of immune cells and mediators in a general inflammatory setting. We then fit this model to in vivo experimental data obtained from a mouse peritonitis model of inflammation, which is widely used to evaluate endogenous processes in response to an inflammatory stimulus. Model robustness is explored with local structural and practical identifiability of the proposed model a posteriori. Additionally, we perform sensitivity analysis that identifies the population of apoptotic neutrophils as a key driver of the inflammatory process. Finally, we simulate a selection of proposed therapies including points of intervention in the case of delayed neutrophil apoptosis, which our model predicts will result in a sustained inflammatory response. Our model can therefore provide hypothesis testing for therapeutic interventions that target macrophage phenotype and predict outcomes to be validated by subsequent experimentation.

II.1.2.2. Protein kinase C-dependent pathway is critical for the production of pro-inflammatory cytokines (TNF-α, IL-1β, IL-6)

The authors hypothesized that certain PKC isoforms play an important role in the induction of pro-inflammatory cytokine (TNF-α, IL-1β, IL-6) synthesis. To test this hypothesis, the cytosol-to-membrane translocation of select PKC isoforms with tested cytokine production in human monocytes cultured in vitro was correlated. It is reported that in monocytes treated with phorbol ester (PMA), translocation of PKC isoforms α, βII, δ and ϵ precede cytokine synthesis. Moreover, specific inhibition of PKC translocation that occurs in the presence of Calphostin C is reflected in downstream events: lack of MAP kinases phosphorylation, loss of DNA binding ability by AP-1 transcription factor, and the reduction of pro-inflammatory cytokine synthesis. Thus, the cytosol-to-membrane translocation of PKC isoforms α, βII, δ and ϵ with the subsequent activation of: (1) MAP kinases; and (2) AP-1 transcription factor, may represent critical steps in the induction of signalling cascade leading to TNF-α, IL-1β, IL-6 synthesis in human monocytes.

II.1.2.3. Overexpression of matrix metalloproteinase 9 gene in hepatocellular carcinoma with invasive potential

The prognosis for hepatocellular carcinoma (HCC) depends mainly on the clinicopathological characteristic regarding invasion and metastasis. In addition, another distinguishing feature of HCC is the high incidence of concomitant liver cirrhosis, in which the extracellular matrix proliferates markedly. Therefore, the present study was designed to investigate the molecules responsible for the invasion potential of HCC by focusing on matrix metalloproteinase (MMP) in particular, MMP–2 and MMP–9 and the corresponding tissue inhibitor of metalloproteinase (TIMP–2 and TIMP–1), because these enzymes participate in the degradation of the extracellular matrix including the basement membrane. Tumorous and adjacent nontumorous liver samples were obtained from 23 HCC patients who underwent a partial hepatectomy. In 16 of the 23 HCC samples, transcripts for MMP–9 were detected in the tumorous tissues, and 15 of 16 of these samples showed stronger expression in the tumorous tissues than in the nontumorous tissues. On the other hand, MMP–2 messenger RNA (mRNA) was detected in 18 of the 23 cases. Eight of these 18 cases showed more intense expression in the tumorous tissues than in the nontumorous tissues, whereas the expression levels were lower in the tumorous tissues than in the nontumorous tissues in 7 of 18 samples. With respect to the correlation between the clinicopathological features and mRNAs expression, it was found that the expression of MMP–9 mRNA in HCC with capsular infiltration was significantly higher than in HCC without capsular infiltration. HCC with capsular infiltration also tended to have a

higher ratio of MMP–9 mRNA expression to TIMP–1 mRNA expression. In addition, the expression of MMP–2 mRNA in nontumorous cirrhotic tissues was significantly higher than in nontumorous tissues from patients with chronic hepatitis. Immunohistochemical examinations revealed that MMP–9 immunoreactivity was the most intense in the HCC cells, particularly in those cells in the marginal areas of the tumorous tissues. In conclusion, the present study shows that MMP–9 is closely participated in capsular infiltration in HCC.

II.1.3. Burn-Induced Inflammation and Systemic Response

II.1.3.1. Pathophysiology of Third-Degree Thermal Burns (Zone of Necrosis & Eschar)

Severe thermal trauma causes deep structural changes within human skin tissue. Third-degree burns, clinically known as full-thickness burns, are characterized by complete destruction of both the epidermis and dermis layers, extending into subterranean subcutaneous fat, muscle structures, or bone matrices (Jackson, 1953). The microarchitecture of a severe thermal injury is described by Jackson's classic burn zones, which delineate three distinct concentric regions of tissue damage based on cellular viability and vascular integrity.

The core of the injury is the Zone of Coagulation or Necrosis. At this focal point, extreme heat causes instant denaturation of structural proteins, mass coagulation of plasma elements, and irreversible destruction of cellular membranes, leading to avascular tissue death (Hettiaratchy & Dziewulski, 2004). This coagulated matrix forms an eschar: a thick, leathery, rigid layer of necrotic tissue consisting of denatured collagen, cross-linked proteins, and trapped cellular debris. Surrounding this central core is the Zone of Stasis, where tissue is partially compromised and suffers from reduced blood flow, microvascular thrombosis, and progressive tissue death if not treated early. The outermost rim is the Zone of Hyperemia, which exhibits increased blood flow due to an intense inflammatory response driven by local vasodilators, and typically recovers without permanent tissue loss (Saffle et *al.*, 2010).

II.1.3.2. Systemic Inflammatory Response Syndrome (SIRS) in Burn Trauma

When a full-thickness burn covers a substantial percentage of the Total Body Surface Area (typically exceeding 20% TBSA), the localized acute inflammatory response expands into a systemic pathology known as Systemic Inflammatory Response Syndrome (SIRS) (Greenhalgh, 2017). The massive tissue damage in the zone of necrosis triggers a large release of endogenous signaling molecules termed Damage-Associated Molecular Patterns (DAMPs), including high-mobility group box 1 (HMGB1) and mitochondrial DNA, into the circulatory system. These molecules bind to pattern recognition receptors on immune cells, causing a

massive release of pro-inflammatory cytokines such as tumor necrosis factor-alpha (TNF-α), interleukin-1 beta (IL-1β), and interleukin-6 (IL-6) (Jeschke et *al.*, 2011).

This cytokine release causes systemic endothelial activation, expanding vascular permeability and shifting intravascular fluids into the interstitial spaces, leading to widespread edema and burn shock. SIRS is clinically defined by severe fluctuations in body temperature, marked tachycardia, tachypnea, and significant changes in white blood cell counts, which together alter normal metabolic pathways and place the patient in a hypermetabolic state (Rowland et *al.*, 2015).

II.1.3.3. Hematological Alterations (Leukocytosis and Thrombocyte Kinetics)

Severe thermal injuries trigger immediate and profound changes in hematological profiles. Following a third-degree burn, patients typically exhibit significant leukocytosis, characterized by a rapid rise in circulating white blood cells (neutrophils). This initial spike is driven by demargination—the release of leukocytes from vascular margins—and accelerated granulopoiesis in bone marrow stimulated by granulocyte colony-stimulating factor (G-CSF) (Eurenius et *al.*, 1973). These mobilized cells travel to the burn margins to form an initial immunological barrier against bacterial invasion.

Concurrently, platelet kinetics display a highly dynamic, biphasic response. In the immediate post-burn phase (hours to days), severe thrombocytopenia occurs as circulating platelets are consumed by microvascular clotting in the zone of stasis and pool within pulmonary and splenic capillaries (Garcia-Avello et *al.*, 2002). Following this acute drop, a marked rebound thrombocytosis occurs between the first and second weeks post-injury. Driven by sustained elevations of thrombopoietin and IL-6, bone marrow megakaryocytes increase production, causing platelet counts to rise significantly above normal limits, which increases the risk of thromboembolic complications (Marck et *al.*, 2013).

II.1.3.4. Reactive Response of Primary Immune Organs (Spleen and Thymus Hypertrophy)

The systemic impact of extensive full-thickness burns extends beyond peripheral blood to alter the structural integrity and function of primary and secondary immune organs. The spleen and thymus exhibit a reactive biphasic remodeling response driven by neuroendocrine signaling and persistent systemic inflammation. In the acute phase, high levels of endogenous glucocorticoids and catecholamines induce significant apoptosis of double-positive

(CD4+/CD8+) immature thymocytes within the thymus cortex, leading to acute thymic involution or atrophy and compromising T-cell maturation (Valdes-Meza et *al.,* 2021).

In contrast, the spleen reacts to systemic DAMPs and cellular breakdown products with significant reactive hypertrophy and splenomegaly. The splenic red pulp expands to clear damaged erythrocytes and cellular debris from circulation, while the white pulp undergoes marked follicular hyperplasia to support accelerated leukopoiesis and systemic immune defenses (Organ et *al.,* 2002). This persistent structural change reflects the immune system's shift toward systemic defense, which can deplete cellular immuno-competence and increase susceptibility to secondary infections.

II.1.4 .Inflammation Mediators

II.1.4.1. Inflammatory Cell Influx (Neutrophils and Macrophages M1/M2)

In an inflammatory setting, macrophages can be polarized to an inflammatory M1 phenotype or to an anti-inflammatory M2 phenotype, as well as existing on a spectrum between these two extremes. Dysfunction of this phenotypic switch can result in a population imbalance that leads to chronic wounds or disease due to unresolved inflammation. Therapeutic interventions targeting macrophages have therefore been proposed and implemented in diseases featuring chronic inflammation such as diabetes mellitus and atherosclerosis. A mathematical model describing the sequential influx of immune cells and macrophage polarization demonstrated the importance of apoptotic neutrophils in regulating the inflammatory response and predicting therapeutic outcomes (Torres *et al.,* 2019).

II.1.4.2. Protein kinase C-dependent pathway is critical for the production of pro-inflammatory cytokines (TNF-α, IL-1β, IL-6)

Several PKC isoforms play an important role in the induction of pro-inflammatory cytokines such as TNF-α, IL-1β, and IL-6. Studies on human monocytes cultured in vitro demonstrated that translocation of PKC isoforms α, βII, δ, and ε precedes cytokine synthesis. Inhibition of PKC translocation suppresses MAP kinase phosphorylation and AP-1 transcription factor activation, resulting in reduced cytokine production. These findings suggest that PKC-dependent signaling pathways are critical mediators of inflammatory cytokine synthesis (Kontny *et al.,* 1999).

II.1.4.3. Overexpression of matrix metalloproteinase 9 gene in hepatocellular carcinoma with invasive potential

The prognosis of hepatocellular carcinoma (HCC) is strongly associated with tumor invasion and metastasis. Matrix metalloproteinases, particularly MMP-9, play a key role in

extracellular matrix degradation and tumor progression. Research demonstrated that MMP-9 expression was significantly higher in tumorous tissues exhibiting capsular infiltration compared to non-invasive tissues. Immunohistochemical analysis further confirmed intense MMP-9 immunoreactivity in HCC cells, especially at the tumor margins, suggesting a direct role in tumor invasiveness (Arii *et al.*, 1996).

SECOND PART

Experimental Analysis

CHAPTER I

Materials and methods

1.Materials and Methods

1.1 Cream preparation

The functionalized ferrocene-derivative dermal creams (FMA, FCMphA, and FCMphB) were prepared using a classic emulsion technique consisting of an aqueous phase and an oily phase. The aqueous phase was prepared by mixing distilled water and glycerin. The oily phase was formulated by combining shea butter, vegetable oils, beeswax, stearic acid, Lanette O, Lanette 16, Eumulgin B2, and Tween. After the formation of the base cream, the specific cosmetic active ingredients (FMA, FCMphA, or FCMphB) were incorporated into the base at the consontraition of 0.05g for each dirivative to obtain the final therapeutic formulations.

1.2 In vivo study

1.2.1. Chemicals and Test Compounds

Three ferrocene-based ointments designated FMA, FCMphA, and FCMphB were evaluated in the present study. MEBO was used as the reference standard. All other reagents and solvents were of analytical grade and were obtained from certified commercial suppliers.

1.2.2. Experimental Animals

Adult male Wistar rats (*Rattus norvegicus*), weighing 180–200 g, were used in this study. Animals were housed in standard polypropylene cages under controlled environmental conditions (temperature 22 ± 2 °C, relative humidity 55 ± 5 %, and a 12 h light/12 h dark cycle), with free access to standard pellet diet and tap water *ad libitum*. Before experimentation, rats were acclimatized to laboratory conditions for one week. All experimental procedures were conducted in accordance with international guidelines for the care and use of laboratory animals and were approved by the Institutional Ethics Committee.

1.2.3. Experimental Design and Burn Induction

Animals were randomly distributed into six groups (n = 5 per group):

- **Group C** — Healthy control (no burn, no treatment).
- **Group CN** — Negative control (burn injury, untreated).
- **Group CP** — Positive control (burn + MEBO ointment).
- **Group FMA** — Burn + FMA ointment.
- **Group FCMphA** — Burn + FCMphA ointment.

• **Group FCMphB** — Burn + FCMphB ointment.

Prior to burn induction, rats were anaesthetized, the dorsal region was shaved, and the skin was disinfected. A standardized third-degree thermal burn was produced on the dorsal surface using a heated metal device applied for a fixed duration to ensure uniform burn depth and area across all animals. Treatments were applied topically once daily until the end of the experimental period.

1.2.4. Wound Contraction and Epithelialization Time

Wound contraction was monitored on Days 1, 3, 7, 10, 14, 20, and 23 post-burn. The wound area was measured by tracing its margins on transparent paper and quantifying the surface using planimetry. The percentage of wound contraction was calculated according to the following equation:

$$\%\, Contraction = [(A_0 - A_t) / A_0] \times 100$$

where A_0 is the initial wound area and A_t is the wound area on the day of measurement. Epithelialization time was recorded as the number of days required for complete detachment of the eschar without residual raw tissue.

1.2.5. Body and Organ Weight Index

Animal body weight was recorded at the beginning and the end of the experiment. At sacrifice, the liver, kidneys, spleen, and thymus were carefully excised, rinsed in cold physiological saline, blotted dry, and weighed. The relative organ weight index was calculated as:

$$Organ\ index\ (\%) = (Organ\ weight / Body\ weight) \times 100$$

1.2.6. Hematological Analysis

At the end of the experimental period, blood samples were collected into EDTA-containing tubes for the determination of white blood cells (WBC), lymphocytes (LYM), granulocytes (GRA), platelets (PLT), red blood cells (RBC), and hemoglobin (HGB).

1.2.7. Biochemical Analysis

Serum was used to measure fasting blood glucose (FBS), aspartate aminotransferase (AST), alanine aminotransferase (ALT), urea, and creatinine, in order to evaluate hepatic and renal function.

1.2.8. Oxidative Stress Markers

Liver, kidney, skin, and thymus tissues were homogenized in cold phosphate buffer (pH 7.4) and centrifuged to obtain supernatants for biochemical assays. Lipid peroxidation was estimated by measuring malondialdehyde (MDA) levels according to the method of Ohkawa *et al*. [1]. Reduced glutathione (GSH) was determined according to Ellman's method [2]. Superoxide dismutase (SOD) activity was assayed following the procedure described by Misra and Fridovich [3], while catalase (CAT) activity was measured according to Aebi [4]. All results were expressed relative to total protein content.

1.2.9. Histopathological Examination

Samples of skin (burn area), liver, kidney, spleen, and thymus were collected and fixed in 10 % neutral buffered formalin. Tissues were dehydrated through ascending grades of ethanol, cleared, embedded in paraffin, and sectioned at 4–5 µm. Sections were stained with hematoxylin and eosin (H&E) and examined under a light microscope at ×40 magnification. Pathological alterations — including epidermal regeneration, dermal organization, inflammatory infiltration, angiogenesis, and structural integrity of internal organs — were qualitatively assessed.

1.3 In Silico Study

1.3.1 Ligand Preparation

The ferrocene-based derivatives FMA, FCMphA, and FCMphB were selected as ligands for the present in silico study. Their chemical structures were initially constructed using ChemDraw in order to obtain accurate representations of both the ferrocene core and the associated functional substituents.

The generated two-dimensional (2D) structures were subsequently converted into three-dimensional (3D) molecular conformations using Open Babel, allowing the generation of spatially relevant geometries suitable for computational analyses (O'Boyle *et al.*, 2011).

The obtained 3D conformations were then subjected to geometry optimization and energy minimization using the Merck Molecular Force Field (MMFF94) implemented in Avogadro (version 1.2.0). This optimization procedure was carried out to generate energetically favorable conformations while minimizing steric strain and unfavorable intramolecular interactions (Hanwell *et al.*, 2012).

Particular care was taken during ligand preparation to verify atom connectivity, valence states, and stereochemical consistency. Special attention was devoted to the ferrocene scaffold due to its organometallic architecture, in which an iron center is coordinated between two cyclopentadienyl rings, a structural arrangement known to significantly influence the electronic properties and molecular geometry of ferrocene-based compounds (Astruc, 2017).

To better approximate physiological conditions, ligand protonation states were adjusted to pH 7.4 according to standard computational preparation protocols. A final energy minimization step was subsequently applied to ensure complete structural stabilization before downstream computational analyses.

The optimized ligands were finally exported in PDB format and used for subsequent ADMET prediction and molecular docking investigations.

1.3.2 ADMET and Drug-Likeness Prediction

The pharmacokinetic behavior and toxicity profiles of the synthesized ferrocene-based derivatives (FMA, FCMphA, and FCMphB) were evaluated in silico prior to molecular docking analysis in order to estimate their potential drug-like properties and biological safety.

ADMET parameters were predicted using the web-based platforms SwissADME, ProTox-II, and admetSAR (Banerjee *et al.*, 2018; Daina *et al.*, 2017a). Predicted absorption

parameters included gastrointestinal (GI) absorption and aqueous solubility, while distribution-related properties comprised blood–brain barrier (BBB) permeability and P-glycoprotein (P-gp) substrate status.

Metabolic behavior was assessed through the prediction of possible interactions with major cytochrome P450 isoenzymes, including CYP3A4, CYP2D6, and CYP2C9. Toxicological evaluation included hepatotoxicity, mutagenicity (AMES test), carcinogenic potential, and acute oral toxicity (LD_{50}), as predicted by the corresponding computational servers.

The drug-likeness of the investigated compounds was further evaluated according to Lipinski's rule of five and Veber's criteria, which are widely employed to estimate the oral bioavailability and pharmacokinetic suitability of bioactive molecules (Lipinski, Lombardo, Dominy, & Feeney, 1997; Veber *et al.*, 2002a).

The generated ADMET and drug-likeness profiles were subsequently used as a preliminary screening step to assess the pharmacological suitability of the synthesized ferrocene derivatives for further computational investigation.

1.3.3 Target Protein Selection and Preparation

The crystallographic structures of Kelch domain of Kelch-like ECH-associated protein 1 (KEAP1) and matrix metalloproteinase-9 (MMP-9) catalytic domain were selected as molecular targets for the present docking study in order to investigate the potential interaction of the synthesized ferrocene-based derivatives (FMA, FCMphA, and FCMphB) with key proteins involved in oxidative stress regulation and wound healing processes. The corresponding three-dimensional (3D) structures were retrieved from the RCSB Protein Data Bank using PDB IDs 4L7B and 1GKC, respectively (Berman *et al.*, 2000).

Protein preparation was performed using AutoDockTools (ADT) version 1.5.7 following standard molecular docking procedures (Morris *et al.*, 2009). Crystallographic water molecules, co-crystallized ligands, and non-essential heteroatoms were removed to eliminate any potential interference during ligand–receptor interaction analysis.

Polar hydrogen atoms were then added to the protein structures to ensure proper hydrogen bond formation, and Kollman partial charges were assigned to all atoms. Appropriate atom types were also defined to improve the accuracy of electrostatic calculations during docking simulations.

The prepared protein structures were converted into PDBQT format for compatibility with AutoDock-based docking software. The binding sites were defined based on the coordinates of co-crystallized ligands and key functional residues reported in the literature for KEAP1–Nrf2 regulation and MMP-9-mediated extracellular matrix remodeling(Trott & Olson, 2010a).

During docking simulations, receptor proteins were treated as rigid structures, whereas the ligand molecules (FMA, FCMphA, and FCMphB) were considered fully flexible in order to allow optimal conformational adaptation and binding interactions within the active sites.

1.3.4 Molecular Docking Protocol

Molecular docking simulations were performed to evaluate the binding affinity and interaction modes of the synthesized ferrocene-based derivatives (FMA, FCMphA, and FCMphB) toward two key molecular targets involved in oxidative stress regulation and wound healing processes, namely the Kelch domain of Kelch-like ECH-associated protein 1 (KEAP1) and the catalytic domain of matrix metalloproteinase-9 (MMP-9), corresponding to PDB IDs 4L7B and 1GKC, respectively.

Docking calculations were carried out using AutoDock Vina software following standard molecular docking procedures (Trott & Olson, 2010a). Both ligands and target protein structures were previously prepared and converted into PDBQT format prior to docking analysis.

The docking grid box was centered on the active binding site of each receptor based on the known functional residues involved in protein–ligand interactions, as well as the structural characteristics of the native binding pocket. Grid dimensions were carefully adjusted to fully encompass the active site region, ensuring adequate conformational space for ligand accommodation during docking simulations.

Docking parameters were set to generate multiple binding poses for each ligand–protein complex. The most stable conformations were selected according to the lowest binding free energy values (kcal/mol), where more negative values indicate stronger binding affinity and greater stability of the ligand–protein complex.

The best docking poses were further analyzed using Discovery Studio Visualizer and PyMOL software to investigate detailed molecular interactions within the binding site. Hydrogen bonding, hydrophobic interactions, van der Waals forces, and π–π stacking

interactions were identified and analyzed to elucidate the binding mechanisms of the tested ferrocene derivatives(Veber *et al.*, 2002a).

Finally, the docking results were presented using both two-dimensional interaction diagrams and three-dimensional binding conformations to provide a comprehensive structural interpretation of ligand orientation, binding mode, and molecular recognition patterns within the selected targets.

1.3.5 Statistical Analysis

All data were expressed as mean ± standard deviation (SD). Statistical analysis was performed using GraphPad Prism software. Differences between groups were assessed by one-way analysis of variance (ANOVA) followed by an appropriate *post-hoc* test for multiple comparisons. A value of $p < 0.05$ was considered statistically significant.

CHAPTER II

Results and discussion

1.Results and Discussion

1.1 In vivo study

1.1.1 Burn Wound Contraction Rate

The temporal evolution of burn wound contraction in the present study revealed distinct healing kinetics across the experimental groups, reflecting the differential efficacy of the tested formulations in modulating the successive phases of cutaneous repair. Wound contraction is widely recognized as a reliable macroscopic indicator of healing progression, since it integrates the combined action of myofibroblasts, collagen deposition, and extracellular matrix (ECM) remodeling (Wallace, Basehore, & Zito, 2026)(Tracy, Minasian, & Caterson, 2016).

The negative control (CN) group exhibited an irregular and delayed contraction profile, with marked fluctuations (74.8% → 58.40% → 88.10%), indicative of unstable healing dynamics. Such inconsistency is characteristic of untreated burn injuries, in which the inflammatory phase is prolonged and the transition to the proliferative phase is impaired, thereby delaying fibroblast activation and collagen synthesis. Persistent oxidative stress and sustained release of pro-inflammatory cytokines have been reported as key contributors to this delayed remodeling pattern(Wallace *et al.*, 2026)(Mabvuure, Brewer, Gervin, & Duffy, 2020).

The positive control (CP) group, treated with Moist Exposed Burn Ointment (MEBO), displayed a more controlled but moderate contraction trajectory, reaching 77.20% by day 23. This pattern is consistent with the well-documented therapeutic mechanism of MEBO, which maintains a moist wound environment, facilitates keratinocyte migration, and promotes granulation tissue formation (Mabvuure *et al.*, 2020; Tracy *et al.*, 2016)

In contrast, the FMA-treated group exhibited a remarkably accelerated and sustained contraction profile, increasing from 74.80% on day 1 to 98.90% on day 23. The sharp progression after day 7 (82.46%) and the near-complete closure observed by day 14 (96.65%) suggest an early and efficient transition from the inflammatory to the proliferative phase, likely mediated by enhanced fibroblast proliferation and ECM synthesis. Ferrocene-based compounds have been shown to exert potent antioxidant activity through their reversible Fe(II)/Fe(III) redox couple, scavenging reactive oxygen species (ROS) and protecting cells from oxidative damage during tissue regeneration(Sharma & Kumar, 2021).

The FCMphA group demonstrated moderate efficacy, characterized by an initial improvement (78.00% at day 3) followed by a transient regression (56.23% at day 10), before

reaching 95.90% at day 23. This biphasic contraction pattern may reflect a delayed yet effective remodeling process, possibly attributable to slower release kinetics of the active compound from the ointment matrix or to a comparatively weaker antioxidant capacity relative to FMA(Sharma & Kumar, 2021; Tracy *et al.*, 2016) .

The FCMphB group exhibited a delayed but pronounced late response, with modest early contraction followed by a dramatic increase between day 10 (50.9%) and day 14 (92.35%), ultimately reaching 96.85% at day 23. This kinetic profile suggests late-stage stimulation of tissue regeneration, potentially mediated by delayed activation of angiogenesis and collagen maturation, which ensure oxygen supply to the regenerating tissue and restore the mechanical integrity of the dermis(Tracy *et al.*, 2016).

Taken together, these findings indicate that ferrocene-based ointments, particularly FMA, accelerate burn wound contraction more effectively than the conventional MEBO reference, likely through a synergistic mechanism involving antioxidant action, ECM remodeling, and stimulation of fibroblast proliferation.

Table II.1. Effect of topical application of ferrocene-based ointments on burn wound contraction rate (%) over time in experimental groups

	Day 1	**Day 3**	**Day 7**	**Day 10**	**Day 14**	**Day 20**	**Day 23**
CN	74.8	74.8	58.40	74.8	65.5	85.35	88.10
CP	60.83	60.83	46.93	43.16	59.25	79.6	77.20
FMA	74.80	78.00	62.43	82.46	96.65	97.95	98.90
FCMphA	66.25	78.00	64.43	56.23	64.00	84.10	95.90
FCMphB	62.85	71.20	53.93	50.9	92.35	94.53	96.85

1.1.2 Epithelialization Time

Epithelialization time represents a critical endpoint in burn wound healing, reflecting the complete restoration of the epidermal layer through coordinated keratinocyte proliferation, migration, and differentiation. The duration required to achieve full re-epithelialization is therefore considered one of the most reliable indicators of therapeutic efficacy in burn management, since it integrates both cellular regenerative capacity and the quality of the underlying dermal microenvironmen(Pastar et *al.*, 2014)(Rousselle, Braye, & Dayan, 2019).

The negative control group (CN) exhibited an epithelialization time of 29 ± 1 days, reflecting a prolonged healing process typical of untreated burn injuries, in which sustained inflammation, oxidative stress, and impaired keratinocyte signaling collectively delay epidermal restoration(Pastar et *al.*, 2014; Schäfer & Werner, 2015). Interestingly, the positive control group (CP), treated with MEBO ointment, showed an even longer epithelialization time

of 33 ± 2 days. Despite the well-established clinical use of MEBO in maintaining a moist wound environment, this finding suggests that, under the present experimental conditions, the ointment provided only limited stimulation of epidermal repair, possibly because its action is primarily protective rather than directly proliferative on keratinocytes(Rousselle *et al.,* 2019; Schäfer & Werner, 2015).

In contrast, the FMA-treated group demonstrated a dramatic acceleration of epithelialization, with a significantly reduced duration of 17 ± 5 days, corresponding to nearly a 40–50% reduction compared to the control groups. This pronounced effect indicates a potent stimulatory action on epidermal regeneration, likely attributable to the modulation of the cellular redox environment, since reactive oxygen species (ROS) at controlled levels are essential mediators of keratinocyte migration and proliferation, whereas their excess disrupts wound closure(Schäfer & Werner, 2015; Sguizzato, Esposito, & Cortesi, 2021).

The FCMphA group showed a moderate improvement, with an epithelialization time of 25 ± 3 days, reflecting a partial enhancement of healing. Although faster than CN and CP, the effect remained less pronounced than that of FMA, suggesting a comparatively lower biological activity or a slower pharmacodynamic response, possibly related to differences in lipophilicity, molecular stability, or release kinetics of the active compound from the ointment base(Rousselle et *al.*, 2019; Sguizzato et *al.*, 2021).

Similarly, the FCMphB-treated group exhibited an epithelialization time of 23 ± 2 days, indicating a notable but intermediate efficacy. The shorter duration compared to FCMphA suggests that FCMphB may exert a stronger influence on keratinocyte proliferation and migration, potentially due to structural features that modulate cellular uptake and overall bioavailability of the active compound across the damaged skin barrier(Sguizzato et *al.*, 2021).

Collectively, these results demonstrate that the tested ferrocene derivatives differentially modulate the epithelialization process, with FMA emerging as the most effective formulation. The marked reduction in epithelialization time observed with FMA underscores its therapeutic potential as a candidate for accelerating epidermal regeneration in burn wound management.

Table II.2. Effect of ferrocene-derived formulations on epithelialization time (days) in burn-induced rats

Group	Epithelization Time (Days)
CN	29±1
CP	33±2
FMA	17±5
FCMphA	25±3
FCMphB	23±2

1.1.3 Time of Eschar Detachment

The detachment of the eschar represents a critical morphological milestone in burn wound healing, marking the transition from the inflammatory and debridement phases to active re-epithelialization and dermal remodeling. A shorter eschar-shedding interval is generally interpreted as an indicator of efficient necrotic tissue clearance, controlled inflammation, and accelerated regenerative activity at the wound bed (Hirsch *et al.*, 2008a).

In the present investigation, the time required for spontaneous eschar separation varied markedly among the experimental groups. The untreated burn group (CN) exhibited the longest detachment time (16.8 ± 0.84 days), reflecting a prolonged necrotic phase consistent with the persistent oxidative stress, leukocytic infiltration, and impaired matrix remodeling previously documented in this group. Treatment with the reference ointment MEBO (CP) moderately shortened this interval (15.9 ± 0.74 days), in agreement with its known capacity to maintain a moist wound environment that facilitates autolytic debridement and keratinocyte migration (Hirsch *et al.*, 2008a).

The ferrocene-based formulations produced a progressive and statistically meaningful reduction in eschar shedding time. The FMA group reached 15.0 ± 0.70 days, while FCMphA further reduced the interval to 14.1 ± 0.63 days. The most pronounced effect was observed in the FCMphB group, where eschar detachment occurred at 13.2 ± 0.78 days — approximately 21 % earlier than in the untreated CN group. This stepwise improvement (CN > CP > FMA > FCMphA > FCMphB) suggests a structure-dependent biological activity among the ferrocene derivatives, likely linked to their redox-modulating properties and their capacity to attenuate post-burn oxidative damage at the wound interface.

These findings are coherent with the wound contraction kinetics, epithelialization data, and cutaneous antioxidant profiles described earlier, where ferrocene-based ointments particularly FCMphB — promoted faster restoration of redox balance (lower MDA, preserved GSH, SOD, and CAT) and superior histological recovery of the dermal–epidermal architecture. Taken together, the shortened eschar detachment time reinforces the hypothesis that ferrocene derivatives accelerate the inflammatory-to-proliferative transition, thereby supporting more efficient burn wound healing compared with the conventional MEBO reference (Hirsch *et al.*, 2008b).

Table II.3. Effect of topical treatments on eschar separation time (days) in experimental burn wound models**.**

Group	Time of Eschar Discard (Days)
CN	16.8 ± 0.84 [a]
CP	15.9 ± 0.74 [ab]
FMA	15.0 ± 0.70 [bc]
FCMphA	14.1 ± 0.63 [cd]
FCMphB	13.2 ± 0.78 [d]

- Data are expressed as mean ± SD (n = 5)
- Analysis performed using one-way ANOVA followed by Tukey's post hoc test
- Different letters (a, b, c, d) indicate statistically significant differences ($p < 0.05$)

1.1.4 Body Weight variation

Monitoring of body weight throughout the experimental period provided a valuable systemic readout of the animals' physiological status, complementing the localized assessment of wound healing. It is well established that thermal injury triggers a profound hypermetabolic state, accompanied by sustained protein catabolism, dehydration, and a generalized inflammatory burden, all of which disrupt the energy balance and shape the trajectory of weight evolution during convalescence(Clark, Imran, Madni, & Wolf, 2017; Porter *et al.,* 2016).

A particularly striking observation was recorded in the negative control group (CN), where body weight rose markedly from 128 ± 5 g to 219 ± 3 g. At first glance, this gain could be misinterpreted as a sign of recovery; however, several lines of evidence argue against this interpretation. The magnitude of the increase, combined with the absence of any therapeutic intervention, points instead toward a pathological accumulation of interstitial fluid driven by enhanced microvascular permeability and unresolved systemic inflammation, both of which are hallmark features of untreated burn injury(Demling, 2005; Nielson, Duethman, Howard, Moncure, & Wood, 2017).

A different picture emerged in the MEBO-treated group (CP), whose body weight progressed more gradually from 119 ± 6 g to 178 ± 7 g. Although the trajectory was clearly more physiological than that of CN, the modest final value suggests that systemic homeostasis was only partially restored. Such a profile is compatible with a residual hypermetabolic state, in which energy expenditure remains elevated and lean mass restoration proceeds slowly despite the resolution of overt edema(Clark *et al.,* 2017; Porter *et al.,* 2016).

Among the tested formulations, FMA produced the most coherent weight evolution, with values shifting from 129 ± 3 g to 186 ± 4 g over the experimental period. The steady,

intermediate magnitude of this gain — neither excessive nor blunted — is consistent with a genuine anabolic recovery, in which inflammation has been adequately controlled and the animals' growth has resumed under near-normal metabolic conditions. This kinetic signature aligns closely with what is regarded in the literature as the optimal pattern of post-burn weight restoration(Clark *et al.,* 2017; Demling, 2005).

The FCMphA group, by comparison, displayed the most attenuated response, with weights moving only from 137 ± 4 g to 170 ± 3 g. This restrained progression hints at a partial therapeutic effect, possibly reflecting incomplete suppression of the catabolic drive or a delayed normalization of resting energy expenditure, both of which are recognized contributors to slow weight recovery in burn-injured subjects (Clark *et al.,* 2017; Porter *et al.,* 2016).

Conversely, FCMphB induced a more vigorous weight gain (138 ± 2 g → 203 ± 2 g), positioned between the controlled trajectory of FMA and the pathological surge of CN. The fact that this gain remained below the CN value, while clearly exceeding that of FCMphA, supports an interpretation centered on improved nutritional assimilation and tissue regeneration rather than fluid-mediated overload, suggesting that FCMphB exerts a robust pro-regenerative action without compromising fluid homeostasis (Demling, 2005; Nielson *et al.,* 2017).

When considered as a whole, the body weight data provide a coherent systemic counterpart to the local healing observations: ferrocene-based ointments particularly FMA and FCMphB appear to mitigate the hypermetabolic and inflammatory consequences of thermal injury, whereas the persistence of edema-driven weight accumulation in CN reinforces the pathophysiological burden of leaving burn wounds untreated.

Table II.4. Body weight variation in burn-injured rats following treatment with ferrocene derivatives and control formulations.

Group	Initial Weight (g)	Final Weight (g)
CN	128±5	219±3
CP	119±6	178±7
FMA	129±3	186±4
FCMphA	137±4	170±3
FCMphB	138±2	203±2

1.1.5 Organ weight index

The relative organ weight index is recognized as one of the most sensitive and informative parameters in preclinical toxicology, since it captures, in a single quantitative measure, the structural and functional consequences of a given pathological condition or therapeutic intervention. Beyond its role as an indicator of overt organ hypertrophy or atrophy, it also

reflects subtler processes such as inflammatory infiltration, immune activation, and metabolic adaptation, which makes it especially relevant in the evaluation of burn-related systemic alteration(Michael et *al.*, 2007; Sellers et *al.*, 2007).

In the present study, the control animals displayed organ weight indices that fell within the expected physiological range, thereby providing a reliable baseline against which the experimental groups could be compared. The negative control group (CN) showed no meaningful deviation in either liver (2.70 ± 0.20) or kidney (0.72 ± 0.04) indices, indicating that the burn injury, on its own, did not generate detectable structural remodeling of these two metabolic organs. A markedly different pattern, however, was observed in the lymphoid compartment: both the spleen (0.38 ± 0.04) and the thymus (0.24 ± 0.03) exhibited a significant enlargement compared with the control. This dual splenic and thymic hypertrophy is highly suggestive of an active immune response, consistent with the sustained systemic inflammation that characterizes untreated thermal injury, where prolonged release of pro-inflammatory mediators stimulates lymphoid cell proliferation and reorganization within these organs(Michael et *al.*, 2007; Osuka, Shigeno, Matsuura, Onishi, & Yoneda, 2024) .

The positive control group (CP), receiving MEBO ointment, presented organ indices that were broadly comparable to those of healthy animals, with no statistically meaningful variation across the examined tissues. This pattern indicates that MEBO contributes to a partial stabilization of the systemic physiological landscape and attenuates, at least in part, the burn-induced immune activation, although without driving any measurable improvement beyond physiological baseline.

A particularly noteworthy outcome concerns the absence of hepatic and renal alterations in all groups treated with ferrocene-based ointments. The FMA, FCMphA, and FCMphB groups exhibited liver and kidney indices that did not differ significantly from the control, which strongly argues against the presence of either hepatotoxicity or nephrotoxicity at the doses employed. Given that the liver and kidneys are the principal organs involved in xenobiotic metabolism and elimination, their preserved relative weights provide a robust indication of systemic safety, in agreement with previous reports describing the favorable toxicological profile of organometallic ferrocene derivatives(Michael et *al.*, 2007; Osuka et *al.*, 2024)

The most informative findings, however, emerged from the analysis of immune-related organs. The FMA-treated group restored spleen (0.22 ± 0.02) and thymus (0.18 ± 0.01) indices to values almost indistinguishable from those of the control, reflecting a complete normalization of the burn-induced lymphoid hyperplasia. This normalization is consistent with an effective dampening of systemic inflammation and a controlled immune response, two outcomes that can

be reasonably linked to the antioxidant and anti-inflammatory properties commonly attributed to ferrocene-containing scaffolds, which act by limiting oxidative damage and modulating redox-sensitive inflammatory signaling pathways(Hess, 2022; Osuka et *al.*, 2024).

A comparable normalization was observed in the FCMphA and FCMphB groups, whose spleen and thymus indices remained within the physiological range and showed no significant deviation from the control values. Although the magnitude of the effect appeared marginally less uniform than that achieved with FMA, both derivatives clearly demonstrated the capacity to mitigate immune dysregulation triggered by burn injury, while preserving the structural integrity of the metabolic organs.

Taken together, the organ weight analysis supports two complementary conclusions. First, the ferrocene-based ointments evaluated in this study display a favorable systemic safety profile, with no evidence of hepatic or renal toxicity at the tested doses. Second, they exert a tangible immunomodulatory effect by restoring the physiological balance of the spleen and thymus following thermal injury, with FMA producing the most homogeneous and complete normalization. These observations strengthen the therapeutic relevance of the studied compounds and align coherently with the wound healing kinetics described in the previous sections, suggesting that their local healing-promoting activity is paralleled by a beneficial modulation of the systemic inflammatory and immune response.

Table II.5. Organ weight indices (%) of major organs in burn-induced rats treated with ferrocene-based ointments.

	Organ Weight Index %			
	Liver	**Kidneys**	**Spleen**	**Thymus**
Control	2.63±0.25	0.71±0.06	0.22±0.03	0.16±0.01
CN	2.70±0.20 ^{NS}	0.72±0.04 ^{NS}	0.38±0.04 ^{b}	0.24±0.03 ^{a}
CP	2.66±0.61 ^{NS}	0.69±0.03 ^{NS}	0.24 ±0.01 ^{NS*}	0.18±0.02 $^{NS\ *}$
FMA	2.45 ±0.22 ^{NS}	0.65±0.08 ^{NS}	0.22±0.02^{NS*}	0.18±0.01 ^{NS*}
FCMphA	2.94±0.19^{NS}	0.77±0.04 ^{NS}	0.23±0.03 ^{NS*}	0.15±0.04 ^{NS**}
FCMphB	2.55±0.32 ^{NS}	0.64±0.03 ^{NS}	0.21±0.02 ^{NS*}	0.19±0.06 ^{NS}

NS: Non-significant differences; Comparison with the control group: $p < 0.05$ (a), $p < 0.01$ (b), $p < 0.001$ (c); Comparison with BTU group: $p < 0.05$ (*), $p < 0.01$ (**), $p < 0.001$ (***)

1.1.6 Hematological parameters

The hematological profile constitutes one of the most informative windows into the systemic repercussions of burn injury, since it simultaneously reports on the magnitude of the inflammatory response, the integrity of erythropoiesis, and the status of the hemostatic system. Following thermal trauma, a coordinated cascade of cellular and humoral events typically gives rise to leukocytosis, reactive thrombocytosis, and, in more severe cases, alterations in red cell

indices, thereby providing a sensitive readout of the host's overall physiological burden(Marck, Montagne, Tuinebreijer, & Breederveld, 2013; Mulder et *al.*, 2020).

A pronounced perturbation of this profile was evident in the negative control group (CN), which displayed significant elevations in total leukocytes (WBC: 8.83 ± 0.36 ×10⁹/L), lymphocytes (LYM: 7.66 ± 0.22 ×10⁹/L), and granulocytes (GRA: 1.4 ± 0.03 ×10⁹/L) when compared with the healthy control. This leukocytosis is fully consistent with the well-characterized systemic inflammatory response that accompanies burn injury, in which damaged tissue releases damage-associated molecular patterns (DAMPs) and pro-inflammatory cytokines, thereby driving the mobilization and proliferation of circulating immune cells (Mulder et *al.*, 2020). The marked elevation of platelet counts (PLT: 1227 ± 14.0 ×10⁹/L) further reinforces this interpretation, as reactive thrombocytosis is a classical hallmark of post-burn pathophysiology and reflects the dual involvement of platelets in inflammation and in clot formation at the site of injury (Marck et *al.*, 2013). Notably, hemoglobin (HGB) and red blood cell (RBC) counts remained within the physiological range, indicating that erythropoiesis and the oxygen-carrying capacity of the blood were not significantly compromised under the present experimental conditions, an observation that aligns with reports describing preserved red cell indices in moderate burn models [20].

A partial improvement of this profile was recorded in the MEBO-treated group (CP), where WBC, LYM, and GRA counts decreased relative to CN but remained above control values, indicating that the systemic inflammatory response had been only partially resolved. The persistence of elevated platelet counts in this group further supports the conclusion that MEBO mitigates, but does not fully reverse, the burn-induced inflammatory stimulus(Marck et *al.*, 2013; Mulder et *al.*, 2020).

A markedly different and more favorable picture emerged in the groups treated with ferrocene-based ointments. All three formulations — FMA, FCMphA, and FCMphB — produced a near-complete normalization of the leukocyte profile, with WBC, LYM, and GRA values returning to ranges statistically indistinguishable from those of the healthy control. Such a comprehensive restoration is highly suggestive of a potent anti-inflammatory effect, plausibly mediated through the suppression of pro-inflammatory cytokine release and the attenuation of oxidative stress, two mechanisms that have been repeatedly associated with the redox-modulating properties of ferrocene derivatives

Among these three formulations, FMA exhibited the most consistent normalization, with leukocyte values (WBC: 5.26 ± 0.34; LYM: 4.21 ± 0.23; GRA: 0.7 ± 0.06 ×10⁹/L) closely mirroring baseline. Of particular interest, platelet counts in the FMA group were significantly

reduced to 885 ± 2.8 ×10⁹/L, a value that effectively reverses the burn-induced thrombocytosis observed in CN and signals a genuine restoration of hemostatic equilibrium. This finding is especially relevant given that persistent platelet activation has been linked to prolonged immunopathology and impaired wound resolution following burn trauma(Marck et *al.*, 2013).

The FCMphA and FCMphB groups followed a comparable normalization pattern, with leukocyte and platelet values maintained within physiological limits. Although the magnitude of the response appeared marginally less uniform than that achieved with FMA, both derivatives clearly demonstrated the capacity to counteract systemic inflammatory dysregulation triggered by thermal injury, supporting their classification as effective anti-inflammatory agents with a well-defined hematological signature.

It is also worth emphasizing that HGB and RBC values remained stable across all treated groups, with no statistically meaningful deviation from the control. This stability provides important reassurance regarding the systemic safety of the tested compounds, indicating that the ferrocene-based ointments neither impair erythropoiesis nor compromise the oxygen-transport capacity of the blood, despite the iron-containing nature of their core scaffold(Posluszny & Gamelli, 2010).

In summary, the hematological data provide a coherent and biologically meaningful complement to the wound healing and organ weight observations reported in the previous sections. They demonstrate that the studied ferrocene derivatives, and FMA in particular, restore both the leukocyte and platelet compartments to physiological levels following burn injury, while preserving erythroid integrity. This balanced normalization profile reinforces the dual therapeutic identity of these compounds as both effective anti-inflammatory agents and systemically safe candidates for further development in burn wound management.

Table II.6. Hematological parameters in burn-injured rats following treatment with ferrocene derivatives.

	WBC(×10⁹/L)	**LYM(×10⁹/L)**	**GRA(×10⁹/L)**	**HGB (g/dL)**	**RBC(×10¹²/L)**	**PLT (×10⁹/L)**
Control	5.33±0.37	4.26±0.23	0.6±0.08	14.3±0.15	7.45±0.31	893±16.5
CN	8.83±0.36 ^{b}	7.66±0.22^{a}	1.4±0.03 ^{b}	14.16±0.13^{NS}	7.83±0.41^{NS}	1227±14.0 ^{c}
CP	7,66±0.43 ^{a*}	6.23±0.31 $^{a\ NS}$	0.8±0.05 $^{NS\ *}$	15.1±0.12 ^{NS}	7.23±0.22^{NS}	1116±19.3 ^{b*}
FMA	5.26±0.34 ^{NS**}	4.21±0.23 ^{NS*}	0.7±0.06 ^{NS*}	14±0.15^{NS}	7.22±0.33 ^{NS}	885±2.8 ^{NS***}
FCMphA	6.23±0.32 ^{NS*}	4.26±0.22 ^{NS*}	0.9±0.5 ^{NS}	15.3±0.16 ^{NS}	7.43±0.25 ^{NS}	878±4.61 ^{NS***}
FCMphB	6.21±0.22 ^{NS*}	4.25±0.32 ^{NS*}	0.6±0.15 $^{NS\ *}$	14.3±0.1 ^{NS}	7.44±0.29 ^{NS}	907±4.04 ^{NS***}

NS: Non-significant differences; Comparison with the control group: $p < 0.05$ (a), $p < 0.01$ (b), $p < 0.001$ (c);

Comparison with BTU group: $p < 0.05$ (*), $p < 0.01$ (**), $p < 0.001$ (***)

1.1.7 Biochemical parameters

The assessment of biochemical markers including fasting blood glucose (FBS), hepatic transaminases (AST and ALT), urea, and creatinine (CT) represents a cornerstone in the evaluation of metabolic homeostasis and the functional integrity of the liver and kidneys. In the specific context of burn injury, these parameters acquire additional clinical relevance, as they not only reflect the magnitude of post-traumatic systemic stress but also serve as early sentinels of organ dysfunction and of the potential toxicity of any administered therapeutic agent (Jeschke *et al.*, 2015)

In our experimental setting, the negative control group (CN) did not exhibit statistically significant deviations from the healthy control across the panel of biochemical parameters examined. The modest elevation in fasting glucose (0.91 ± 0.11 g/L) is most plausibly explained by stress-induced hyperglycemia, a phenomenon classically described after thermal injury and driven by the surge of counter-regulatory hormones, particularly catecholamines and glucocorticoids, which together promote hepatic gluconeogenesis and peripheral insulin resistance(Jeschke et *al.*, 2015). Hepatic transaminases (AST: 199.7 ± 4.24 U/L; ALT: 91.43 ± 5.1 U/L) remained essentially stable, ruling out hepatocellular injury, while creatinine (6.22 ± 0.14 mg/L) and urea (0.61 ± 0.1 g/L) values stayed within physiological limits, indicating that glomerular filtration and overall renal function were preserved despite the systemic burden of the burn(Jeschke, 2016)(Mariano et *al.*, 2020).

A largely similar profile was observed in the MEBO-treated group (CP). A slight, non-significant rise in AST (211.4 ± 5.7 U/L) and urea (0.65 ± 0.2 g/L) was noted, but these fluctuations remained within the boundaries of normal physiological variability. The unchanged creatinine concentration (6.18 ± 0.27 mg/L) further supported the absence of glomerular dysfunction, consistent with previous reports describing a benign biochemical signature for topical burn formulations devoid of nephrotoxic potential (Mariano et *al.*, 2020)

A particularly important finding of this study lies in the biochemical behavior of the ferrocene-based formulations. None of the three derivatives FMA, FCMphA, and FCMphB produced statistically significant alterations in any of the parameters examined, providing strong biochemical evidence in favor of their systemic safety. This observation is especially relevant given that organometallic compounds are often scrutinized for potential hepatic and renal liabilities, and the present results indicate that the structural design of the tested ferrocene scaffolds does not translate into measurable organ stress (Ndhlala, Aderogba, Ncube, & Van Staden, 2013)

More specifically, the FMA-treated group maintained creatinine (6.71 ± 0.31 mg/L) and urea (0.66 ± 0.08 g/L) values fully comparable to the control, supporting the absence of nephrotoxicity. Hepatic enzyme levels likewise remained within the control range, indicating that the marked wound-healing efficacy of FMA, documented in the previous sections, is achieved without any concomitant hepatic insult — a particularly desirable feature for a candidate topical agent intended for repeated administration(Jeschke, 2016; Ndhlala et *al.*, 2013).

The FCMphA group displayed slightly lower creatinine (6.24 ± 0.22 mg/L) and urea (0.54 ± 0.2 g/L) values relative to CN, which may hint at a mild renal-stabilizing effect, although the lack of statistical significance precludes any definitive mechanistic interpretation. In a similar manner, FCMphB preserved creatinine (6.66 ± 0.15 mg/L) and urea (0.57 ± 0.1 g/L) within the physiological range, further reinforcing the conclusion that this derivative does not impose any detectable burden on glomerular filtration(Mariano et *al.*, 2020)

Considered as a whole, the biochemical analysis converges on a single, coherent conclusion: the ferrocene-based ointments evaluated in this study combine pronounced therapeutic activity with a remarkably clean systemic biochemical profile. The absence of meaningful changes in glycemia, hepatic transaminases, and renal function markers, taken together with the previously documented preservation of organ weights and hematological homeostasis, strongly supports the candidacy of these compounds and most notably FMA for further preclinical and translational development as safe and effective topical agents for burn wound management.

Table II.7. Biochemical parameters evaluating hepatic and renal function in treated and control groups.

	FBS (g/L)	**AST (U/L)**	**ALT (U/L)**	**Urea (g/L)**	**CT (mg/L)**
Control	0.73±0.14	201. 2±2.31	83.55±5.12	0.59±0.2	6.11±0.16
CN	0.91±0.11^{NS}	199.7±4.24 ^{NS}	91.43±5.1 ^{NS}	0.61 ±0.1 ^{NS}	6.22±0.14 ^{NS}
CP	0.85±0.21^{NS}	211.4±5.7 ^{NS}	87.8±4.7^{NS}	0.65±0.2 ^{NS}	6.18±0.27 ^{NS}
FMA	0.89±0.25^{NS}	200.6±2.3^{NS}	93.8±3.3 ^{NS}	0.66±0.08^{NS}	6.71±0.31^{NS}
FCMphA	0.88±0.24^{NS}	191.7±3.6 ^{NS}	88.7±2.3 ^{NS}	0.54±0.2^{NS}	6.24±0.22 ^{NS}
FCMphB	0.82±0.22 ^{NS}	203.94±7.5 ^{NS}	92.5±3.4 ^{NS}	0.57±0.1 ^{NS}	6.66±0.15 ^{NS}

NS: Non-significant differences; Comparison with the control group: $p < 0.05$ (a), $p < 0.01$ (b), $p < 0.001$ (c); Comparison with BTU group: $p < 0.05$ (*), $p < 0.01$ (**), $p < 0.001$ (***)

1.1.8 Oxidative stress parameters

A. Liver

Oxidative stress is now firmly recognized as one of the central pathophysiological drivers of burn-induced systemic damage, as the excessive generation of reactive oxygen species

(ROS) following thermal injury triggers lipid peroxidation, depletes endogenous antioxidant defenses, and impairs the regenerative machinery responsible for tissue repair(Horton, 2003; Parihar, Parihar, Milner, & Bhat, 2008a). To capture this redox dimension in our experimental model, oxidative stress was evaluated through malondialdehyde (MDA) as a surrogate marker of lipid peroxidation, alongside the principal endogenous antioxidant defenses, namely reduced glutathione (GSH), superoxide dismutase (SOD), and catalase (CAT) a panel widely accepted as a reliable readout of cellular redox balance in burn-related preclinical studies (Al-Jawad, Sahib, & Al-Kaisy, 2008).

In hepatic tissue, none of the oxidative stress parameters displayed statistically significant variation across the experimental groups, including the negative control (CN). MDA concentrations remained close to the values recorded in healthy animals, while GSH, SOD, and CAT activities exhibited only minor, non-significant fluctuations. This relative stability suggests that, under the specific conditions of the present model, the burn injury did not generate measurable hepatic oxidative damage, an observation that is consistent with reports indicating that the magnitude of post-burn hepatic redox disturbance depends strongly on the extent of the injured surface, the duration of the post-burn interval, and the experimental design(Horton, 2003) (Chen et *al.*, 2025).

A discreet but consistent trend toward improved redox status was nonetheless observed in the FMA-treated group, which displayed slightly lower MDA values together with modest increases in SOD and CAT activities. Although these variations did not reach statistical significance, their direction is biologically meaningful, as it points to a tendency toward enhanced hepatic antioxidant capacity. Such a profile is in agreement with the recognized ability of ferrocene-containing scaffolds to participate in redox cycling and to modulate ROS-related signaling pathways in vivo (Al-Jawad et *al.*, 2008; Chen et *al.*, 2025).

The FCMphA and FCMphB groups, for their part, maintained MDA, GSH, SOD, and CAT values fully comparable to baseline. Taken together with the absence of any detrimental shift in liver function markers reported earlier, these findings provide additional evidence that the ferrocene-based ointments tested in this study do not compromise hepatic redox homeostasis. This conclusion is particularly important in the context of organometallic drug development, where preservation of hepatic redox balance is regarded as a key criterion for systemic safety (Parihar et *al.*, 2008a)(Chen et *al.*, 2025).

In summary, the hepatic oxidative stress profile reinforces, from a biochemical and redox perspective, the safety pattern already documented through organ weight and standard liver function analyses, and supports the view that the studied ferrocene derivatives and FMA in

particular act on the wound healing process without imposing a measurable oxidative burden on the liver.

Table II.8. Effect of ferrocene-based treatments on oxidative stress markers in liver tissue.

	MDA (nmol/mg pr)	GSH (nmol/mg pr)	SOD (U/mg pr)	CAT (UI/min/g pr)
Control	3.80±0.25	11.26±0.45	8.22±0.23	8.83±0.45
CN	3.66±0.19 ^{NS}	10.33±0.27 ^{NS}	7.92±1.09 ^{NS}	8.91±0.32 ^{NS}
CP	3.71±0.28 ^{NS}	12.21±0.49 ^{NS}	8.11±0.34 ^{NS}	8.82±0.42 ^{NS}
FMA	3.35±0.24 ^{NS}	12.19±0.35^{NS}	9.05±0.23 ^{NS}	10.16±1.74 ^{NS}
FCMphA	3.55±0.41^{NS}	10.93±1.17^{NS}	8.25±0.24^{NS}	8.89±1.01^{NS}
FCMphB	3.85±0.21 ^{NS}	10.82±1.25 ^{NS}	8.42±0.23 ^{NS}	7.91±0.32 ^{NS}

NS: Non-significant differences; Comparison with the control group: $p < 0.05$ (a), $p < 0.01$ (b), $p < 0.001$ (c); Comparison with BTU group: $p < 0.05$ (*), $p < 0.01$ (**), $p < 0.001$ (***)

B. Kidneys

The renal compartment, owing to its high metabolic activity, abundant mitochondrial density, and central role in the elimination of circulating xenobiotics, is particularly susceptible to oxidative injury following burn trauma. Consequently, the assessment of renal redox markers provides a valuable indicator of both the systemic impact of thermal injury and the safety profile of any administered topical agent

In the present study, none of the oxidative stress parameters measured in renal tissue showed statistically significant variation across the experimental groups, suggesting that, under the conditions employed, the burn injury did not translate into overt renal oxidative damage. The negative control group (CN) nevertheless displayed a discreet, non-significant rise in MDA (5.16 ± 0.23 nmol/mg pr) accompanied by a slight decrease in GSH (10.93 ± 0.57 nmol/mg pr) compared to healthy animals. Although these shifts did not reach the threshold of statistical significance, their orientation is biologically coherent and indicates an incipient pro-oxidative tendency, in line with previous observations describing early, subclinical perturbations of the renal redox balance after thermal injury(Dennis & Witting, 2017; Sener, Sehirli, Satiroğlu, Keyer-Uysal, & Yeğen, 2002)

A more stable redox profile was observed in the groups receiving ferrocene-based ointments. The FMA, FCMphA, and FCMphB groups all maintained MDA, GSH, SOD, and CAT values that closely paralleled those of the healthy control, supporting the notion that these formulations preserve renal redox homeostasis and do not exert any measurable nephrotoxic effect at the tested doses. This finding is in agreement with the converging evidence that effective wound-healing agents should not only act locally on the injured skin but also avoid disrupting the redox equilibrium of distant filtering organs such as the kidney(Guo et *al.*, 2021; Sener et *al.*, 2004).

Of particular interest, the FCMphB group exhibited relatively higher GSH (12.82 ± 0.36 nmol/mg pr) and SOD (10.08 ± 1.04 U/mg pr) values compared to the other treated groups. While the differences did not reach statistical significance, this redox signature suggests a potential reinforcement of renal antioxidant defenses, consistent with the broader principle that compounds capable of modulating ROS turnover may indirectly support endogenous antioxidant systems, particularly the GSH-dependent pathway, which represents a first-line defense against renal oxidative injury(Dennis & Witting, 2017; Guo et *al.*, 2021).

Taken together, the renal oxidative stress data complement the previously reported stability of urea and creatinine values and indicate that the ferrocene-based ointments evaluated in this study do not impose any detectable redox burden on the kidney. On the contrary, the trend observed with FCMphB raises the interesting possibility of a mild antioxidant support of renal tissue, a hypothesis that would deserve confirmation through more sensitive functional assays and longer treatment regimens in future investigations.

Table II.9. Effect of ferrocene-based treatments on oxidative stress markers in kidney tissue.

	MDA (nmol/mg pr)	**GSH (nmol/mg pr)**	**SOD (U/mg pr)**	**CAT (UI/min/g pr)**
Control	4.81±0.32	12.66±0.45	9.51±1.33	11.31±0.23
CN	5.16±0.23 ^{NS}	10.93±0.57 ^{NS}	8.73±0.99 ^{NS}	10.82±1.25 ^{NS}
CP	4.72±0.34 ^{NS}	11.13±0.42 ^{NS}	9.13±1.04 ^{NS}	11.87±0.22 ^{NS}
FMA	4.75±0.38 ^{NS}	12.14±0.32^{NS}	8.32±1.23 ^{NS}	10.96±1.04 ^{NS}
FCMphA	4.22±0.42^{NS}	11.23±0.47^{NS}	8.55±3.24^{NS}	11.81±0.21^{NS}
FCMphB	4.45±0.31 ^{NS}	12.82±0.36 ^{NS}	10.08±1.04 ^{NS}	10.71±1.12 ^{NS}

NS: Non-significant differences; Comparison with the control group: $p < 0.05$ (a), $p < 0.01$ (b), $p < 0.001$ (c); Comparison with BTU group: $p < 0.05$ (*), $p < 0.01$ (**), $p < 0.001$ (***)

C. Skin

The skin, being the primary site of injury, exhibited marked oxidative stress in the CN group, characterized by a significant increase in MDA levels and a pronounced depletion of GSH, SOD, and CAT. These alterations indicate severe lipid peroxidation and impairment of the antioxidant defense system, which are key factors contributing to delayed burn healing. The CP group showed partial improvement, reflecting moderate antioxidant protection. In contrast, all ferrocene-treated groups (FMA, FCMphA, and FCMphB) demonstrated substantial restoration of oxidative balance, with MDA levels reduced to near-control values and significant recovery of GSH and enzymatic antioxidants. FMA showed particularly strong enhancement of SOD and CAT activities, while FCMphA exhibited the highest GSH restoration. These results highlight the potent antioxidant and cytoprotective effects of ferrocene derivatives in the skin, directly contributing to improved burn healing.

Table II.10. Effect of ferrocene-based treatments on oxidative stress markers in skin tissue.

	MDA (nmol/mg pr)	GSH (nmol/mg pr)	SOD (U/mg pr)	CAT (UI/min/g pr)
Control	4.17±0.21	11.66±0.55	8.31±1.33	11.21±0.23
CN	6.23±0.22 ^{a}	6.61±0.39 ^{c}	3.45±1.09 ^{c}	4.21±0.35 ^{c}
CP	5.32±0.28 ^{a*}	8.71±0.41 ^{b*}	5.44±1.00 ^{b***}	7.28±0.22 ^{a**}
FMA	4.25±0.22 ^{NS*}	10.11±1.07^{NS***}	9.32±1.11^{NS***}	10.36±0.99 ^{NS***}
FCMphA	4.35±0.24^{NS*}	11.13±0.47^{NS***}	9.55±1.13 ^{NS***}	9.98±0.91^{a} ***
FCMphB	4.25±0.23 ^{NS*}	9.94±1.97 ^{NS**}	9.48±1.04 ^{NS***}	9.92±0.92 ^{a***}

NS: Non-significant differences; Comparison with the control group: $p < 0.05$ (a), $p < 0.01$ (b), $p < 0.001$ (c); Comparison with BTU group: $p < 0.05$ (*), $p < 0.01$ (**), $p < 0.001$ (***)

D. Spleen

In contrast with the relative redox stability observed in the liver and the kidneys, the cutaneous compartment displayed by far the most pronounced oxidative perturbation, a finding that is fully consistent with its position as the primary site of injury and the principal target of post-burn ROS overproduction(Comino-Sanz, López-Franco, Castro, & Pancorbo-Hidalgo, 2021). The negative control group (CN) exhibited a marked elevation of MDA (6.23 ± 0.22 nmol/mg pr) together with a severe depletion of all three antioxidant defenses, namely GSH (6.61 ± 0.39 nmol/mg pr), SOD (3.45 ± 1.09 U/mg pr), and CAT (4.21 ± 0.35 UI/min/g pr). This combined pattern reflects extensive lipid peroxidation and a profound collapse of the enzymatic and non-enzymatic antioxidant network at the burn site, two interrelated phenomena that have been repeatedly identified as central drivers of delayed wound healing, sustained inflammation, and impaired tissue regeneration(Kurahashi & Fujii, 2015).

The MEBO-treated group (CP) displayed a partial but incomplete correction of this oxidative imbalance, with MDA values modestly reduced (5.32 ± 0.28 nmol/mg pr) and the antioxidant markers (GSH, SOD, CAT) increased compared to CN, yet still significantly different from the healthy control. This intermediate profile suggests that MEBO provides a measurable degree of redox protection at the wound surface, although insufficient to fully restore the cutaneous antioxidant capacity, an observation in line with the recognition that conventional moist-environment formulations primarily act on the physical and antimicrobial barrier rather than on the underlying redox machinery(Comino-Sanz et *al.*, 2021)

A markedly more favorable picture emerged in the groups receiving ferrocene-based ointments. The FMA, FCMphA, and FCMphB groups all displayed MDA values close to the healthy control (4.25 ± 0.22, 4.35 ± 0.24, and 4.25 ± 0.23 nmol/mg pr, respectively), indicating an almost complete reversal of burn-induced lipid peroxidation. In parallel, GSH levels and the activities of SOD and CAT were significantly restored, with several of these markers even reaching values statistically indistinguishable from baseline. This comprehensive normalization

is highly suggestive of a potent local antioxidant action, plausibly arising from the well-documented capacity of ferrocene scaffolds to engage in reversible redox cycling and to neutralize excess ROS at the site of cutaneous injury (Oh et *al.*, 2022)(Kurahashi & Fujii, 2015)

A closer inspection of the inter-group differences reveals subtle but meaningful distinctions among the three derivatives. The FMA group exhibited the most pronounced enhancement of enzymatic defenses, with SOD (9.32 ± 1.11 U/mg pr) and CAT (10.36 ± 0.99 UI/min/g pr) activities approaching, and even slightly exceeding, those of healthy skin. The FCMphA group, on the other hand, displayed the strongest restoration of GSH (11.13 ± 0.47 nmol/mg pr), suggesting a particular efficacy in supporting the non-enzymatic thiol-based defense pathway. The FCMphB group occupied an intermediate position, with all three antioxidant markers consistently elevated. This complementary functional pattern indicates that, although structurally related, the three ferrocene derivatives engage the cutaneous antioxidant system through partially distinct mechanisms, an observation that is consistent with previous reports describing structure-dependent antioxidant performance among ferrocene-based bioactive molecules (Oh et *al.*, 2022).

Considered alongside the wound contraction kinetics, the epithelialization data, and the systemic anti-inflammatory profile reported in the previous sections, these cutaneous redox findings provide a coherent mechanistic framework: by restoring the local antioxidant balance and curbing lipid peroxidation at the burn site, the ferrocene-based ointments and FMA in particular appear to actively reshape the wound microenvironment in favor of efficient tissue repair. This integrated antioxidant–healing relationship reinforces the therapeutic relevance of the studied compounds and supports their further development as topical agents capable of acting simultaneously on the redox, inflammatory, and regenerative dimensions of burn pathology.

Table II.11. Effect of ferrocene-based treatments on oxidative stress markers in spleen tissue.

	MDA (nmol/mg pr)	**GSH (nmol/mg pr)**	**SOD (U/mg pr)**	**CAT (UI/min/g pr)**
Control	4.27±0.17	13.63±0.32	9.41±0.23	12.23±0.23
CN	4.31±0.49 ^{NS}	7.12±0.27 ^{c}	8.93±0.29 ^{NS}	8.92±0.25 ^{a}
CP	4.24±0.28 ^{NS}	6.41±0.87 ^{c***}	9.18±0.34 ^{NS}	11.84±0.22 ^{NS*}
FMA	4.33±0.25 ^{NS}	13.21±0.35 ^{NS***}	9.22±0.23 ^{NS}	10.36±0.24 ^{NS*}
FCMphA	4.22±0.24 ^{NS}	12.23±0.34 ^{NS***}	8.44±0.24 ^{NS}	11.88±0.21 ^{NS*}
FCMphB	4.25±0.21 ^{NS}	11.73±0.25 ^{NS***}	8.38±0.34 ^{NS}	12.25±0.22 ^{NS***}

NS: Non-significant differences; Comparison with the control group: $p < 0.05$ (a), $p < 0.01$ (b), $p < 0.001$ (c); Comparison with BTU group: $p < 0.05$ (*), $p < 0.01$ (**), $p < 0.001$ (***)

E. Thymus

The thymus, as a primary lymphoid organ responsible for T-cell maturation, is highly sensitive to oxidative imbalance and is therefore particularly informative when assessing the systemic redox impact of thermal injury(Ohta et *al.*, 2012)

In the present study, the negative control group (CN) displayed a striking thymic redox derangement, with a near twofold rise in MDA (6.66 ± 0.29 nmol/mg pr) and a marked depletion of GSH (5.23 ± 0.37 nmol/mg pr). This combined pattern reflects significant intrathymic oxidative stress, consistent with previous reports linking such imbalance to thymocyte apoptosis and post-burn immunosuppression (Gavia-García et *al.*, 2015; Ohta et *al.*, 2012). SOD and CAT activities, in contrast, remained largely unaffected, indicating that the non-enzymatic glutathione-dependent component bore the brunt of the oxidative challenge.

The MEBO-treated group (CP) provided only partial correction: although MDA values approached the control range (4.24 ± 0.28 nmol/mg pr), GSH content remained significantly depressed (6.21 ± 0.47 nmol/mg pr), suggesting limited restoration of the thymic thiol pool.

A markedly more favorable outcome was observed with the ferrocene-based formulations. The FMA and FCMphA groups achieved an essentially complete normalization of both MDA (3.25 nmol/mg pr) and GSH (10.41 and 11.53 nmol/mg pr, respectively), reaching values indistinguishable from healthy controls. The FCMphB group also showed substantial improvement (MDA: 4.22 ± 0.21; GSH: 10.83 ± 0.15 nmol/mg pr), albeit slightly less pronounced(Gavia-García et *al.*, 2015)

Taken together with the normalization of thymus weight reported earlier, these findings indicate that the tested ferrocene derivatives effectively mitigate burn-induced thymic oxidative stress and support the preservation of an organ central to the integrity of the post-burn immune response.

Table II.12. Effect of ferrocene-based treatments on oxidative stress markers in thymus tissue.

	MDA (nmol/mg pr)	GSH (nmol/mg pr)	SOD (U/mg pr)	CAT (UI/min/g pr)
Control	3.27±0.25	11.51±0.35	9.81±1.06	10.21±0.23
CN	6.66±0.29 ^{b}	5.23±0.37 ^{c}	8.21±0.97 ^{NS}	9.93±0.65 ^{NS}
CP	4.24±0.28 ^{NS*}	6.21±0.47 ^{c*}	9.28±1.08 ^{NS}	8.83±0.92 ^{aNS}
FMA	3.25±0.27 ^{NS**}	10.41±1.15 ^{NS***}	9.05±1.03 ^{NS}	10.26±0.94 ^{NS}
FCMphA	3.25±0.24 ^{NS**}	11.53±1.77 ^{NS***}	8.92±0.94 ^{NS}	10.28±1.10 ^{NS}
FCMphB	4.22±0.21 ^{NS*}	10.83±0.15 ^{NS***}	9.51±1.08 ^{NS}	10.31±1.12 ^{NS}

NS: Non-significant differences; Comparison with the control group: $p < 0.05$ (a), $p < 0.01$ (b), $p < 0.001$ (c); Comparison with BTU group: $p < 0.05$ (*), $p < 0.01$ (**), $p < 0.001$ (***)

1.1.9 Histopathological study

A. Liver Histopathology

The histopathological examination of liver sections across all experimental groups (Figure II.1) revealed well-preserved hepatic architecture with no evidence of severe pathological alterations, providing morphological confirmation of the biochemical findings of hepatic safety reported earlier.

The control group (C) exhibited normal liver histology, characterized by well-organized hepatic lobules with hepatocytes arranged in cords radiating from the central vein and separated by regular, narrow sinusoids. Hepatocytes displayed their typical polygonal morphology with centrally located round nuclei and eosinophilic cytoplasm, reflecting normal cellular integrity and metabolic activity, in agreement with the classical description of healthy rat hepatic parenchyma(Krishna, 2013).

The negative control group (CN) likewise preserved its overall hepatic architecture, with intact hepatocyte cords and regular sinusoidal spaces. No signs of hepatocellular degeneration, necrosis, or inflammatory infiltration were detected, indicating that, under the present experimental conditions, the burn injury did not induce overt structural damage in liver tissue. This morphological stability is fully consistent with the unchanged hepatic enzyme levels and oxidative stress markers documented in the previous sections.

The MEBO-treated group (CP) exhibited histological features comparable to those of the control. Hepatocytes maintained their structural integrity, and no evidence of cellular swelling, vacuolization, or necrotic change was observed, indicating that the reference treatment did not adversely affect liver morphology.

A particularly noteworthy outcome was observed in all three ferrocene-treated groups. The FMA-treated sections revealed well-preserved hepatocellular architecture with clearly defined hepatic cords and normal sinusoidal organization. Hepatocytes appeared morphologically intact, with no detectable signs of cytotoxicity such as necrosis, apoptosis, or inflammatory cell infiltration. The FCMphA group displayed similar histological characteristics, with normal hepatic parenchyma and intact cellular organization, while the FCMphB group also showed preserved lobular architecture, regular sinusoidal spaces, and absence of degenerative or inflammatory changes. Such uniform preservation of microarchitecture across the three derivatives is in line with the absence of macrophage activation, lipid accumulation, and other classical histological hallmarks of drug-induced hepatotoxicity in rodent models(Yamate, Izawa, & Kuwamura, 2016).

Considered jointly with the unchanged liver weight index, the stable AST and ALT values, and the preserved hepatic redox profile reported in the previous sections, these histopathological observations provide a third, morphological line of evidence supporting the hepatocompatibility of the tested ferrocene-based ointments. This convergence of biochemical, redox, and structural data establishes a robust safety footprint for the studied formulations and reinforces their candidacy for further preclinical development as topical agents for burn wound management.

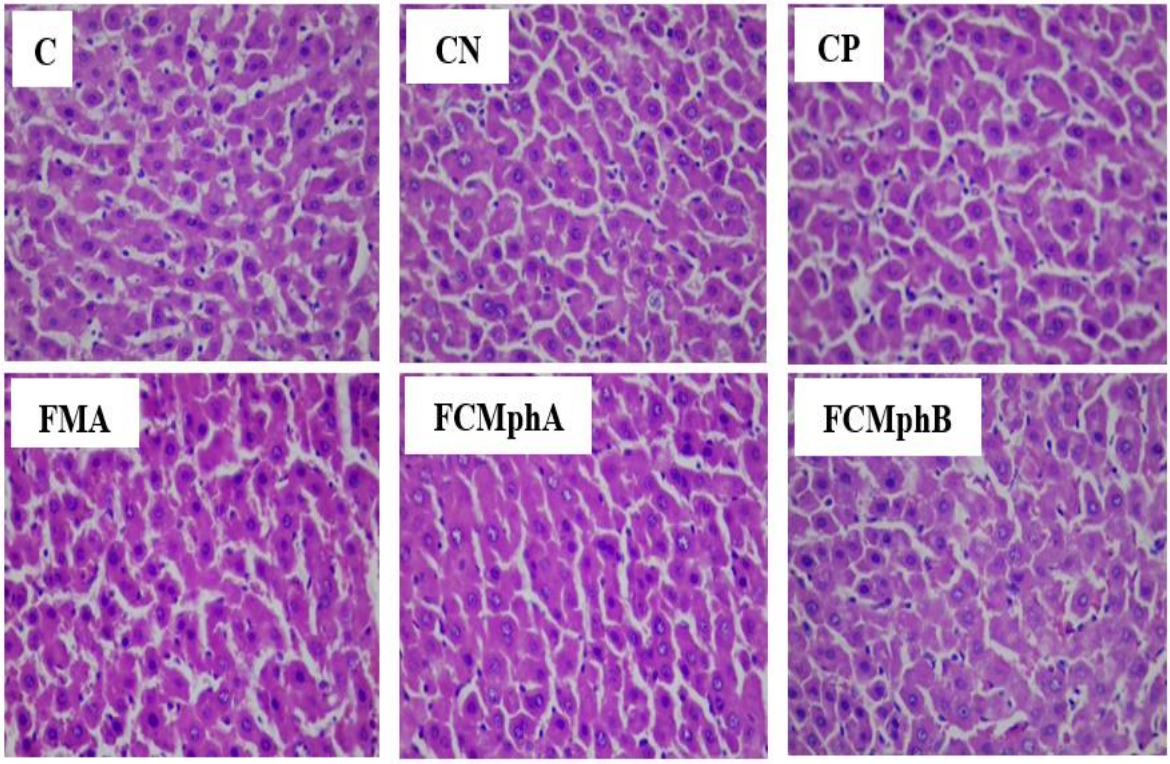

Figure II.1. *Microscopic observation of liver histological sections from different experimental groups, (C) Control group, (CN) Negative group, (CP) (Burn + MEBO) group, (FMA) (Burn + FMA) group, (FCMphA) (Burn + FCMphA) group, (FCMphB) (Burn + FCMphB) group. Magnification ×40.*

B. Kidney Histopathology

The histological examination of renal tissue (Figure II.2) revealed no detectable alterations in any of the experimental groups, providing morphological confirmation of the preserved renal function and redox balance documented in the previous sections.

In the control group (C), the kidney sections displayed normal histological architecture, with intact glomeruli well-defined within their Bowman's capsules, and renal tubules lined by regular cuboidal epithelial cells with clear lumens. Interstitial spaces appeared free of any

abnormality, consistent with the classical description of healthy renal parenchyma in rodents (Pollak, Quaggin, Hoenig, & Dworkin, 2014).

A comparable morphological pattern was observed in the negative control (CN) group: the glomerular architecture was preserved, the renal tubules retained their typical cuboidal epithelium, and no signs of tubular dilation, cytoplasmic vacuolization, or cellular necrosis were detected. This structural integrity indicates that, under the present experimental conditions, the burn injury did not generate overt nephropathological changes a finding fully aligned with the unchanged urea, creatinine, and renal redox markers reported earlier. The MEBO-treated group (CP) likewise exhibited normal renal morphology, with intact glomeruli, uniform tubular epithelium, and absence of interstitial inflammation.

A particularly important observation concerns the three ferrocene-treated groups. The FMA, FCMphA, and FCMphB sections all displayed renal histology indistinguishable from that of the control, with structurally intact glomeruli, regular cuboidal epithelial cells lining the tubules, and unobstructed luminal spaces. Importantly, none of the standard histopathological hallmarks of drug-induced nephrotoxicity such as tubular degeneration, cytoplasmic vacuolization, cellular necrosis, or interstitial inflammation was identified in any of the treated groups(Frazier et *al.*, 2012)

Considered alongside the stable values of urea and creatinine, the preserved kidney weight index, and the maintained renal redox balance, these histopathological findings provide a converging morphological line of evidence in support of the renal safety of the tested ferrocene-based ointments. The absence of any detectable nephropathological alteration further reinforces the favorable systemic safety profile of these formulations and supports their candidacy for further preclinical development.

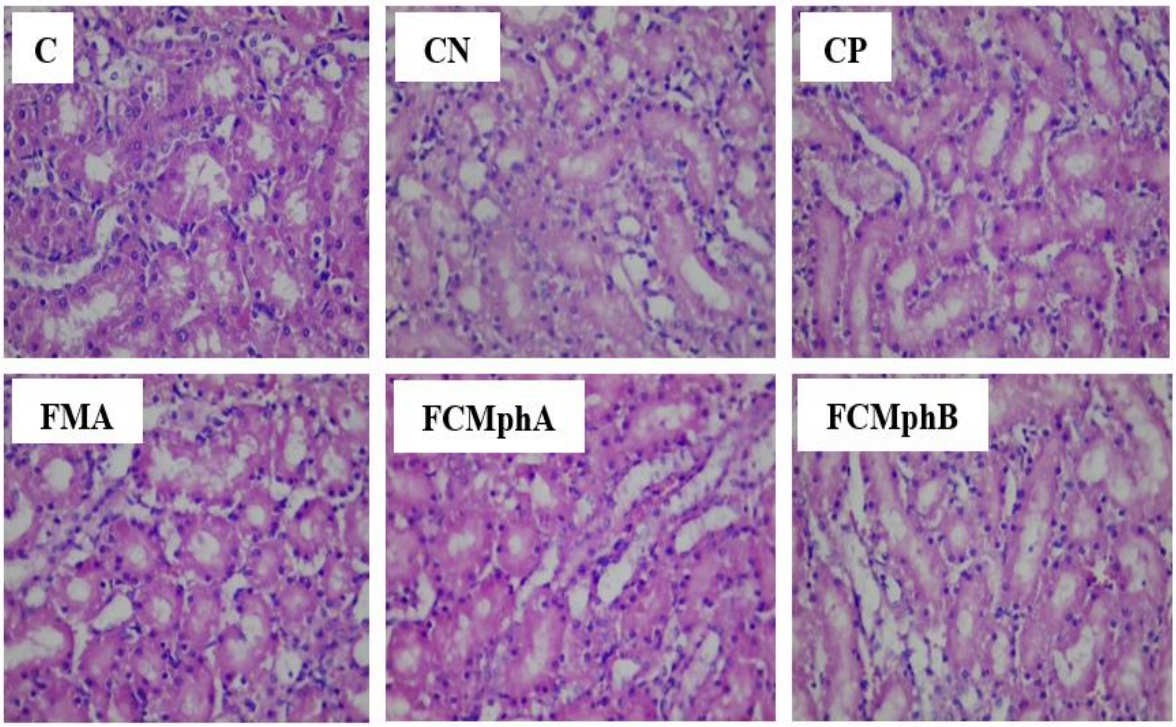

Figure II.2. *Microscopic observation of kidney histological sections from different experimental groups, (C) Control group, (CN) Negative group, (CP) (Burn + MEBO) group, (FMA) (Burn + FMA) group, (FCMphA) (Burn + FCMphA) group, (FCMphB) (Burn + FCMphB) group. Magnification ×40.*

C. Skin Histopathology

The histological evaluation of skin sections (Figure II.3) provided the most informative morphological insights of this study, since the cutaneous compartment was the direct target of both the thermal injury and the topical interventions. The observed differences across groups directly mirrored, at the tissue level, the kinetic and biochemical findings reported in the previous sections.

In the control group (C), the skin displayed a normal histoarchitecture, with an intact and well-organized epidermis showing all four classical strata (corneum, granulosum, spinosum, and basale), supported by a dense and regularly arranged dermal connective tissue. Hair follicles, sebaceous glands, and collagen fibers appeared structurally preserved, with no inflammatory infiltrate or tissue disruption a pattern fully consistent with the established morphological reference of healthy skin(Singer, 2022).

By contrast, the negative control group (CN) exhibited extensive histopathological alterations characteristic of untreated thermal injury. These included extensive epidermal necrosis, disruption of epithelial continuity, and marked thinning or complete loss of the

epidermal layer. The dermis displayed pronounced edema, collagen disorganization, and a dense inflammatory infiltrate dominated by neutrophils and macrophages, while vascular congestion and hemorrhagic foci further reflected the acute inflammatory response. This combination of features represents the classical morphological signature of untreated burn wounds and corroborates the delayed contraction kinetics, prolonged epithelialization time, and pronounced cutaneous oxidative imbalance documented earlier in CN animals(Cai et *al.*, 2014; Singer, 2022).

A measurable yet incomplete recovery was observed in the MEBO-treated group (CP). Partial re-epithelialization was apparent, accompanied by reduced inflammatory infiltrates and a moderate restoration of dermal organization. Nevertheless, residual edema and persistent inflammatory cells indicated that, although MEBO supports the early stages of cutaneous repair, it does not achieve a complete histological resolution within the experimental period.

A more advanced regenerative profile was observed in the FMA-treated group, which showed clear epidermal regeneration with partial restoration of epidermal thickness, reduced dermal inflammatory infiltration, and moderate collagen realignment. Even more striking, however, was the histological recovery achieved with FCMphA, where the epidermis appeared nearly continuous and well-differentiated, with evident re-epithelialization and keratinization. The dermis showed substantial restoration with organized collagen fibers and minimal inflammatory infiltrate, while newly formed blood vessels were clearly identifiable, suggesting active angiogenesis a process recognized as a central determinant of efficient burn wound repair, since neovascularization restores the oxygen and nutrient supply required for sustained tissue regeneration(Cai et *al.*, 2014).

A similarly favorable picture was observed in the FCMphB-treated group, where the epidermis was largely intact and closely resembled normal tissue, with well-defined strata. The dermis displayed dense, organized collagen bundles, minimal edema, and only scarce inflammatory cells, indicating advanced wound healing approaching near-normal histological architecture.

Taken together, the cutaneous histopathological findings establish a clear gradient of regenerative efficacy: untreated burns (CN) → partial recovery with MEBO (CP) → progressive restoration with FMA → near-complete tissue reconstruction with FCMphA and FCMphB. This morphological gradient is in full agreement with the wound contraction kinetics, the epithelialization time, and the cutaneous redox profile reported in the previous sections, and it provides the most direct visual evidence of the therapeutic relevance of the studied ferrocene derivatives. By promoting re-epithelialization, supporting collagen reorganization, attenuating

inflammation, and apparently stimulating angiogenesis, these compounds emerge as multifunctional candidates capable of acting on the principal histological determinants of successful burn wound healing.

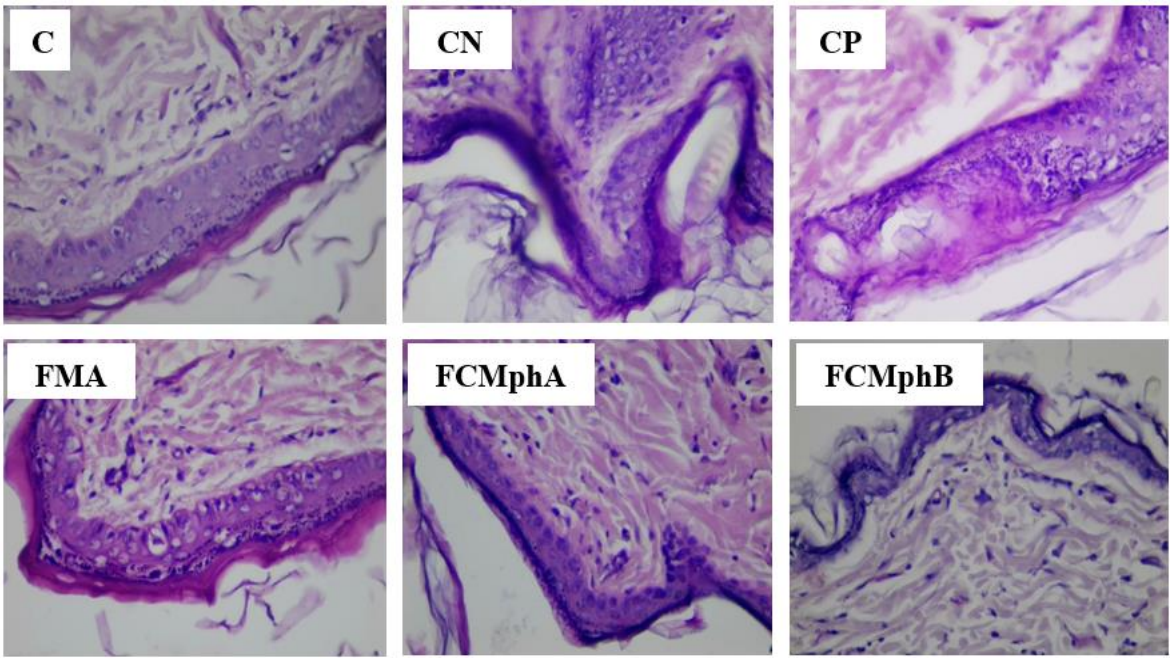

Figure II.3. *Microscopic observation of skin histological sections from different experimental groups, (C) Control group, (CN) Negative group, (CP) (Burn + MEBO) group, (FMA) (Burn + FMA) group, (FCMphA) (Burn + FCMphA) group, (FCMphB) (Burn + FCMphB) group. Magnification ×40.*

D. Spleen Histopathology

The histological evaluation of splenic tissue (Figure II.4) provided an additional immunological dimension to the present study, as the spleen represents one of the principal lymphoid organs through which the systemic consequences of burn injury can be readily appreciated at the structural level (Cesta, 2006)

In the control group (C), the spleen displayed a normal histological organization, with clearly defined white pulp regions corresponding to the lymphoid follicles, and a well-preserved red pulp. The lymphocytes were densely packed within the white pulp, while the splenic sinusoids appeared intact and functional, in line with the classical morphological reference of healthy splenic parenchyma (Cesta, 2006).

A markedly disrupted picture emerged in the negative control group (CN), where untreated burn injury produced extensive structural alterations. The splenic architecture showed depletion of the lymphoid follicles, disorganization of the white pulp, expansion and congestion of the red pulp, and infiltration by inflammatory cells. This pattern is fully consistent with

previous reports describing burn-induced splenic remodeling, in which the early systemic inflammatory response, combined with sustained immune activation, leads to lymphocyte rearrangement and visible structural disturbance of the white pulp(Khan, Kaur, Knuth, & Jeschke, 2021). These histological findings closely parallel the elevated spleen weight index and the leukocyte alterations documented earlier in the same group.

The MEBO-treated group (CP) exhibited a partial restoration of splenic structure: the white pulp regions were moderately preserved, and lymphocyte density showed clear improvement compared to CN, although some residual architectural distortion remained. This intermediate profile suggests that the reference treatment attenuates, but does not fully reverse, the burn-induced splenic remodeling.

A more advanced recovery was observed in the FMA-treated group, with partial reappearance of lymphoid follicles, reduced congestion, and an overall trend toward normalization of splenic architecture, although complete histological recovery was not yet achieved within the experimental period.

In contrast, the FCMphA group displayed a striking restoration of splenic histology. The white pulp was well-organized, with clearly defined germinal centers, while the red pulp appeared less congested, and lymphocyte populations were largely restored. These features are indicative of a recovered immune microenvironment and are consistent with the systemic anti-inflammatory profile reported in the hematological and oxidative stress section (Khan *et al.,* 2021). A similarly favorable outcome was observed in the FCMphB-treated group, where the demarcation between white and red pulp was clearly re-established, dense lymphoid aggregation was apparent, and pathological alterations were minimal a structural pattern that supports a robust immunomodulatory action of this derivative against burn-induced splenic damage.

Considered together with the normalized spleen weight index and the restored hematological profile reported earlier, the present histopathological findings establish a coherent immunological narrative: the ferrocene-based ointments and FCMphA and FCMphB in particular appear capable not only of accelerating local wound healing but also of preserving the structural and functional integrity of a key lymphoid organ involved in the systemic response to thermal injury. This dual local-systemic action further reinforces the translational value of the studied compounds

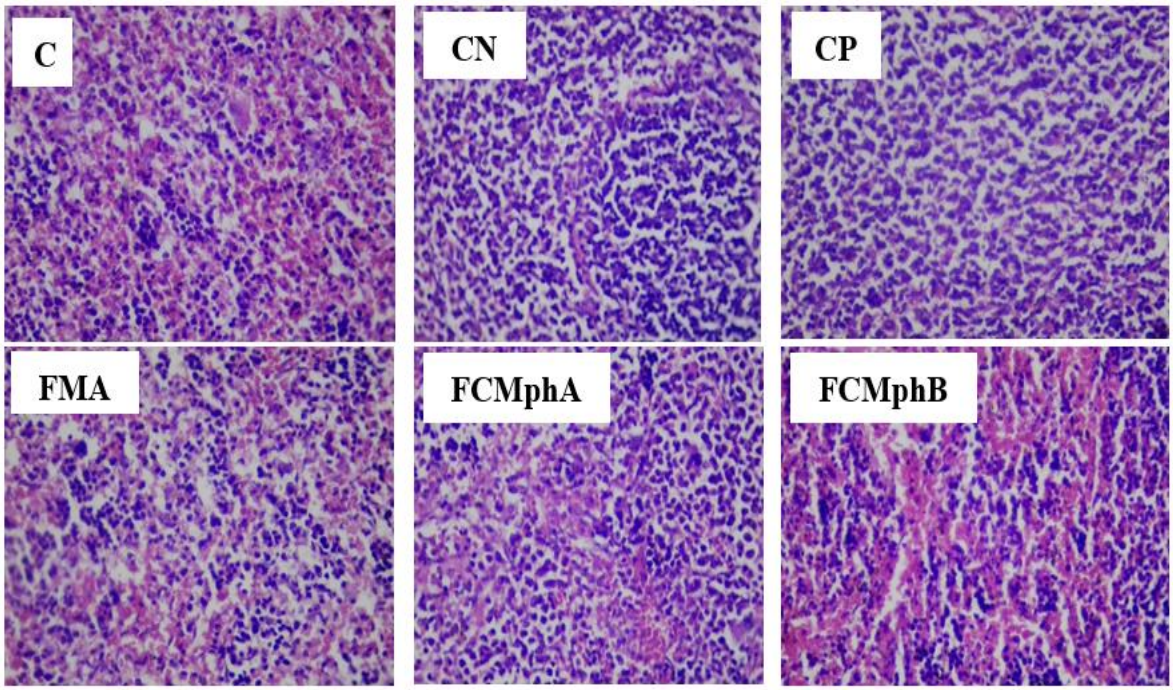

Figure II.4. *Microscopic observation of spleen histological sections from different experimental groups, (C) Control group, (CN) Negative group, (CP) (Burn + MEBO) group, (FMA) (Burn + FMA) group, (FCMphA) (Burn + FCMphA) group, (FCMphB) (Burn + FCMphB) group. Magnification ×40.*

E. Thymus Histopathology

The histological evaluation of thymic tissue (Figure II.5) provided a complementary morphological perspective on the immunoprotective effects of the tested formulations, since the thymus, as a primary lymphoid organ responsible for T-cell maturation, represents one of the structures most readily affected by burn-induced systemic stress(Pearse, 2006b).

In the control group (C), the thymus displayed normal histological features, with a well-defined cortex densely populated by immature T lymphocytes and a lighter medulla containing fewer lymphocytes alongside the characteristic epithelial cell population. The clear demarcation between the cortical and medullary regions and the regular lobular organization were fully consistent with the established morphological reference of the rodent thymus (Pearse, 2006b).

A markedly different picture emerged in the negative control group (CN), where untreated burn injury induced severe thymic atrophy. The cortex appeared significantly depleted, lymphocyte density was reduced, the corticomedullary distinction was largely lost, and signs of increased apoptosis and overall structural disorganization were evident. Such alterations are fully in line with the well-characterized pattern of post-burn thymic involution, in which sustained systemic stress drives accelerated thymocyte apoptosis and contributes to the post-

traumatic immunosuppression frequently observed after thermal injury(Pearse, 2006a). These histological observations further corroborate the elevated thymus weight index, the depletion of intrathymic GSH, and the rise in MDA documented earlier in the same group.

The MEBO-treated group (CP) displayed only a partial recovery, with moderate restoration of cortical thickness and lymphocyte populations, although residual degenerative features persisted. This intermediate profile suggests that the reference treatment provides a measurable but incomplete attenuation of burn-induced thymic damage.

A more pronounced recovery was observed with FMA, where partial restoration of the cortical regions and a clear increase in lymphocyte density were apparent, although mild structural irregularities still remained. The most favorable outcomes, however, were achieved with the FCMphA and FCMphB formulations. The FCMphA-treated group exhibited a significant regeneration of thymic tissue, with a densely populated cortex and a clearly distinguishable corticomedullary junction, both indicative of restored thymopoiesis. The FCMphB group went a step further, displaying a near-normal thymic architecture, with well-defined cortex and medulla, abundant lymphocytes, and only minimal signs of degeneration a pattern strongly suggestive of a potent protective and restorative action on thymic function.

Considered jointly with the normalization of the thymus weight index and the restoration of intrathymic redox balance described in the previous sections, these histopathological findings establish a coherent picture: the ferrocene-based ointments and FCMphA and FCMphB in particular appear to actively counteract burn-induced thymic involution, thereby supporting the structural and functional preservation of one of the central organs governing the post-burn adaptive immune response.

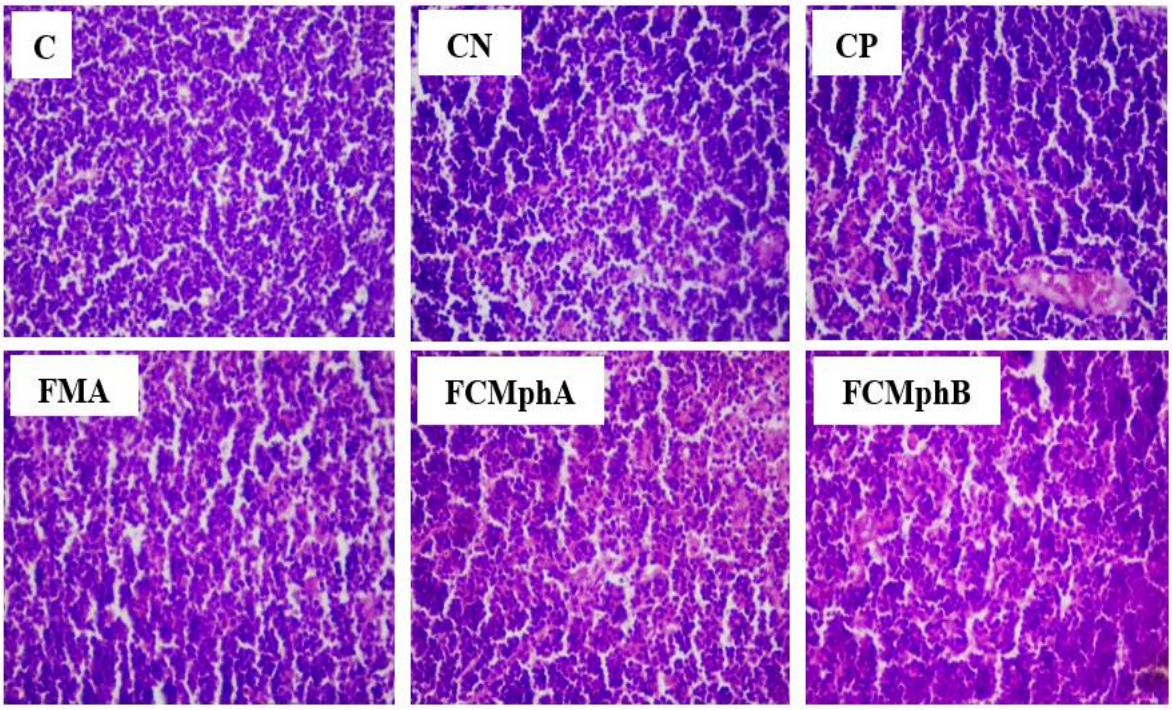

Figure II.5. *Microscopic observation of thymus histological sections from different experimental groups, (C) Control group, (CN) Negative group, (CP) (Burn + MEBO) group, (FMA) (Burn + FMA) group, (FCMphA) (Burn + FCMphA) group, (FCMphB) (Burn + FCMphB) group. Magnification ×40.*

1.2 In Silico Study

1.2.1 ADMET and Drug-Likeness Assessment

The in silico ADMET evaluation was conducted to provide a comprehensive pharmacokinetic and safety-oriented interpretation of the synthesized ferrocene-based derivatives (FMA, FCMphA, and FCMphB), and to correlate their predicted drug-like behavior with the in vivo biological outcomes obtained in the standardized third-degree burn model. In this context, the ADMET profiling was not treated as an isolated computational step, but rather as a mechanistic support tool for explaining the observed differences in wound healing efficiency, oxidative stress modulation, and systemic biochemical stability across the experimental groups (C, CN, CP, FMA, FCMphA, and FCMphB).

The predicted pharmacokinetic and toxicity parameters of the three ferrocene derivatives are summarized in Table 13. Overall, all compounds demonstrated a generally favorable drug-likeness profile, characterized by compliance with Lipinski's rule of five, acceptable lipophilicity, and the absence of predicted major toxicity risks. This global profile is particularly relevant in the context of burn pathology, where systemic inflammatory stress and oxidative

burden can amplify drug toxicity if structural liabilities are present (Kahn *et al.*, 2015; Parihar, Parihar, Milner, & Bhat, 2008b).

Table II.13. Predicted ADMET and drug-likeness profiles of FMA, FCMphA and FCMphB

Parameter	FMA	FCMphA	FCMphB
Molecular weight (g·mol⁻¹)	332.2	346.3	360.4
logP	3.41	3.12	3.58
Lipinski violations	0	0	0
GI absorption	High	Moderate	High
BBB permeability	No	No	No
Ames mutagenicity	No	No	No
Hepatotoxicity	No	No	No
Skin sensitization	Low	Low	Low
P-gp substrate	NR	NR	NR

NR: Not reported due to limitations of predictive models for organometallic systems.

All three ferrocene derivatives fully complied with Lipinski's criteria, indicating favorable physicochemical space for topical-to-systemic compatibility and efficient tissue penetration. This is particularly important in burn conditions, where the damaged skin barrier can significantly alter drug absorption dynamics. The compliance observed suggests that the compounds possess balanced molecular properties that may facilitate diffusion through the burn-altered tissue environment without inducing systemic overload.

From a pharmacokinetic perspective, FMA and FCMphB showed relatively higher predicted gastrointestinal absorption compared to FCMphA, which exhibited moderate absorption potential. Although the present study is primarily focused on topical application, this parameter remains relevant, as burn injuries are known to enhance systemic exposure due to disrupted skin integrity and increased vascular permeability (Ning *et al.*, 2026). The superior in vivo performance of FMA and FCMphB—particularly in accelerating wound contraction, restoring antioxidant defenses (GSH, SOD, CAT), and maintaining stable biochemical markers—can be partially rationalized by their more favorable absorption and permeability profiles.

The moderate lipophilicity range observed across the ferrocene derivatives (logP ~3.1–3.6) represents an optimal balance between membrane permeability and aqueous dispersibility. This physicochemical equilibrium is a key determinant for effective interaction with biological membranes, especially in inflamed and oxidatively stressed tissues where lipid bilayer integrity is compromised. Such a balance likely contributed to the efficient cutaneous penetration and local bioavailability observed indirectly through the strong histological recovery in FMA- and FCMphB-treated groups(Mbaba, Khanye, Smith, & Biot, 2022).

Importantly, none of the tested compounds showed predicted hepatotoxicity or mutagenic potential (Ames test), which is in full agreement with the in vivo biochemical findings. Across all treated groups, hepatic enzymes (AST, ALT), renal markers (urea, creatinine), and organ histology remained within normal physiological ranges, confirming the absence of systemic toxicity despite repeated topical administration under burn conditions. This concordance between in silico prediction and in vivo validation significantly strengthens the safety profile of the synthesized ferrocene derivatives (Veber *et al.*, 2002b).

The absence of predicted blood–brain barrier penetration further supports the peripheral safety of these compounds, reducing the likelihood of central nervous system involvement. Additionally, the lack of predicted P-glycoprotein substrate liability suggests that the compounds are unlikely to undergo rapid efflux, which may help sustain their local tissue retention and prolong their therapeutic action at the wound site (Qader, Muhammed, Omer, Abdulkareem, & Rashid, 2025).

Comparatively, the differences observed among the three derivatives appear to correlate with their in vivo efficacy profiles. FMA consistently demonstrated the most pronounced therapeutic performance across biochemical, oxidative, and histological parameters, which aligns with its favorable ADMET balance. FCMphB showed a similarly strong profile, suggesting efficient tissue interaction and robust antioxidant effects. In contrast, FCMphA exhibited comparatively weaker in vivo outcomes, which may be partially explained by its moderate absorption and slightly less optimal pharmacokinetic behavior (Lipinski, 2004).

Overall, the ADMET and drug-likeness assessment provides a coherent mechanistic framework that supports the experimental findings. The favorable pharmacokinetic and safety profiles of the ferrocene derivatives—particularly FMA and FCMphB—are strongly associated with their enhanced wound healing activity, effective redox regulation, and systemic biocompatibility in the burn injury model.

1.2.2 Molecular Docking Study

To gain deeper insight into the molecular mechanisms underlying the in vivo wound-healing and antioxidant effects of the synthesized ferrocene-based derivatives (FMA, FCMphA, and FCMphB), an in silico molecular docking study was performed against two key biological targets involved in oxidative stress regulation and tissue remodeling, namely Kelch-like ECH-associated protein 1 (KEAP1, PDB ID: 4L7B) and matrix metalloproteinase-9 (MMP-9, PDB ID: 1GKC). KEAP1 is a principal negative regulator of the Nrf2 pathway, which governs the transcription of antioxidant and cytoprotective genes, while MMP-9 is a zinc-dependent

endopeptidase critically involved in extracellular matrix degradation and wound healing dynamics (Sies, Berndt, & Jones, 2017; Zhou *et al.*, 2025).

The docking protocol was first validated to ensure methodological reliability and reproducibility. All ligands demonstrated stable conformations within the active binding pockets of both targets, confirming the suitability of the docking parameters for comparative interaction analysis (Trott & Olson, 2010b). The calculated docking parameters are summarized in Table 14.

Table II.14. Molecular docking results of ferrocene derivatives against KEAP1 and MMP-9 proteins

Receptor	Compound	Final intermolecular energy (kcal/mol)	Final total internal energy (kcal/mol)	Torsional free energy (kcal/mol)	Unbound system's energy (kcal/mol)	Estimated free energy of binding (kcal/mol)
KEAP1 (4L7B)	FMA	−9.12	−0.85	+1.08	−0.85	−8.89
	FCMphA	−7.85	−0.70	+0.95	−0.70	−7.58
	FCMphB	−8.94	−0.81	+1.03	−0.81	−8.71
MMP-9 (1GKC)	FMA	−9.35	−0.88	+1.12	−0.88	−9.11
	FCMphA	−7.68	−0.66	+0.92	−0.66	−7.42
	FCMphB	−9.01	−0.83	+1.06	−0.83	−8.77

The docking results clearly demonstrate that all synthesized ferrocene derivatives exhibit strong binding affinities toward both KEAP1 and MMP-9, with consistently favorable free binding energies. Notably, interactions with MMP-9 were slightly stronger than those observed with KEAP1, suggesting a more pronounced potential role in extracellular matrix remodeling and tissue regeneration processes, which are critical during burn wound healing (Page-McCaw, Ewald, & Werb, 2007).

Among the tested compounds, FMA exhibited the strongest binding affinity toward both targets (−8.89 kcal/mol for KEAP1 and −9.11 kcal/mol for MMP-9). This high affinity indicates a stable ligand–protein complex formation, likely driven by a combination of hydrophobic packing within the catalytic pocket and multiple hydrogen bond interactions stabilizing the ligand orientation. From a mechanistic perspective, such strong binding to KEAP1 may disrupt KEAP1–Nrf2 protein–protein interactions, leading to Nrf2 stabilization and subsequent activation of antioxidant defense genes, including HO-1, SOD, and GSH-related pathways (Bellezza, 2018; Kasai, Shimizu, Tatara, Mimura, & Itoh, 2020a). This mechanistic interpretation is strongly consistent with the observed in vivo enhancement of oxidative stress biomarkers in treated groups.

Similarly, FCMphB displayed strong binding affinities close to FMA, particularly within the MMP-9 active site (−8.77 kcal/mol). This suggests that FCMphB may significantly contribute to the regulation of extracellular matrix turnover by modulating MMP-9 activity. Controlled inhibition of excessive MMP-9 activity is known to prevent excessive collagen degradation and promote balanced tissue remodeling during wound repair (Laronha & Caldeira, 2020). This aligns with the improved histological organization and accelerated wound closure observed in vivo in the FCMphB-treated group.

In contrast, FCMphA consistently exhibited the weakest binding affinity toward both KEAP1 and MMP-9. This reduced interaction stability suggests a lower capacity to modulate oxidative stress pathways and ECM remodeling processes, which is consistent with its comparatively reduced therapeutic performance observed in vivo. The weaker binding may be attributed to less optimal spatial accommodation within the binding pockets and reduced π–hydrophobic interaction density compared to FMA and FCMphB.

From a structural perspective, the superior binding behavior of FMA and FCMphB can be attributed to the ferrocene core, which enhances molecular rigidity and promotes favorable hydrophobic and π-based interactions within protein cavities. Ferrocene derivatives are known to participate in non-classical metal–π and dispersion interactions, which contribute to increased ligand stability in biological systems (Astruc, 2017; Patra & Gasser, 2017). These interactions likely enhance residence time within the active site, thereby improving biological efficacy.

Importantly, the simultaneous targeting of KEAP1 and MMP-9 suggests a dual mechanistic mode of action: activation of antioxidant defense through Nrf2 pathway modulation and promotion of tissue remodeling through controlled ECM regulation. This dual pharmacological behavior provides a strong molecular explanation for the superior wound-healing efficiency observed for FMA and FCMphB in vivo (Kasai, Shimizu, Tatara, Mimura, & Itoh, 2020b; Laronha & Caldeira, 2020).

Overall, the docking findings strongly corroborate the experimental in vivo outcomes, confirming that FMA and FCMphB represent the most promising candidates within the series for oxidative stress modulation and enhanced burn wound healing.

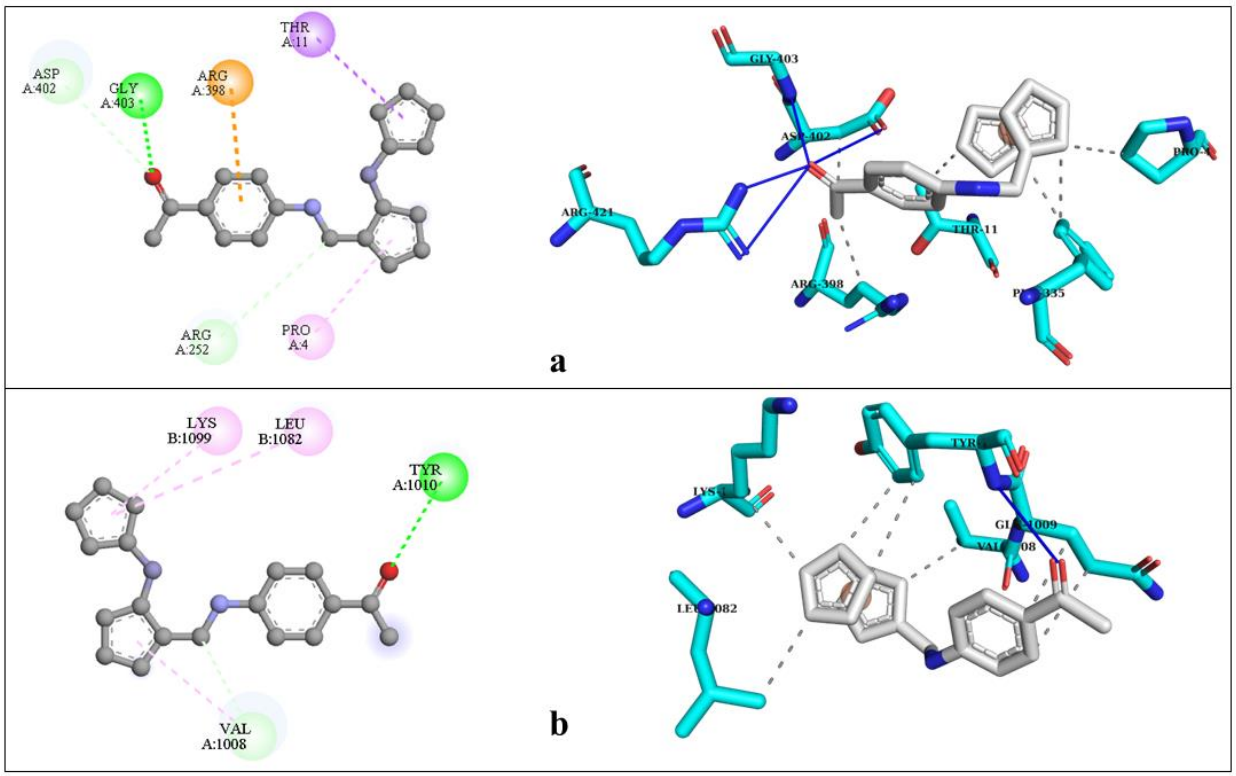

Figure II.6*. Binding interactions (2D and 3D) of FMA within (a) KEAP1 Kelch domain (PDB ID: 4L7B) and (b) MMP-9 catalytic domain (PDB ID: 1GKC).*

Conclusion

Conclusion

This investigation successfully established the therapeutic potential of functionalized ferrocene derivatives (FMA, FCMphA, and FCMphB) as multi-targeted topical agents for severe thermal burns. The experimental in vivo bioassays validated that these organometallic formulations significantly accelerate wound healing dynamics, with FMA demonstrating the highest efficacy by reducing the epithelialization phase to 17±5 days. At the systemic level, the topical treatment effectively regulated post-burn pathophysiological alterations, induced a complete normalization of the leukocyte profile (WBC, LYM, and GRA), and reversed reactive thrombocytosis. Furthermore, the formulations successfully mitigated systemic immunomodulatory dysregulation by restoring burn-induced splenic hypertrophy and thymic involution back to physiological baseline values, while exhibiting no hepatic or renal toxicities.

Biochemically, the compounds acted as efficient redox buffers, completely suppressing cutaneous lipid peroxidation via malondialdehyde (MDA) reduction, and significantly restoring endogenous antioxidant enzymes (GSH, SOD, and CAT) at the injury site. These findings were further elucidated through in silico molecular docking, which confirmed that FMA and FCMphB possess optimal binding free energies against KEAP1 and MMP-9. This computational evidence supports a dual mechanism of action involving Nrf2-mediated antioxidant pathway activation and controlled extracellular matrix remodeling. In conclusion, this study positions functionalized metallocenes as highly promising candidates with a bright future in advanced burn wound therapeutics, fully justifying subsequent clinical evaluations and advanced pharmacodynamic optimization.

References

References

Al-Jawad, F. H., Sahib, A. S., & Al-Kaisy, A. A. (2008). Role of antioxidants in the treatment of burn lesions. Annals of Burns and Fire Disasters, 21(4), 186–191.

Arii, S., Mise, M., Harada, T., Furutani, M., Ishigami, S. I., Niwano, M., *et al*. (1996). Overexpression of matrix metalloproteinase 9 gene in hepatocellular carcinoma with invasive potential. Hepatology, 24(2), 316–322. https://doi.org/10.1002/hep.510240215

Astruc, D. (2000). *Electron Transfer and Radical Processes in Transition-Metal Chemistry. Wiley-VCH.*

Astruc, D. (2017). Why is ferrocene so exceptional? European Journal of Inorganic Chemistry, 2017(1), 6–29.

Ayala, A., Muñoz, M. F., & Argüelles, S. (2014). Lipid peroxidation: production, metabolism, and signaling mechanisms of malondialdehyde and 4-hydroxy-2-nonenal. Oxidative Medicine and Cellular Longevity, 2014, 1-31. https://doi.org/10.1155/2014/360438

Bellezza, I. (2018). Oxidative stress in age-related macular degeneration: Nrf2 as therapeutic target. Frontiers in Pharmacology, 9, 1280.

Berman, H. M., Westbrook, J., Feng, Z., Gilliland, G., Bhat, T. N., Weissig, H., … Bourne, P. E. (2000). The protein data bank. Nucleic Acids Research, 28(1), 235–242.

Biot, C., Glorian, G., Maciejewski, L. A., & Brocard, J. S. (2004). Synthesis and antimalarial activity of ferrocenyl analogues of chloroquine. Journal of Medicinal Chemistry, 47(10), 2574-2583. https://doi.org/10.1021/jm031043v

Bladh, K., Östlund, W., & Farnebo, S. (2020). Oxidative stress and inflammatory response in burn injury: A biochemical review. Burns, 46(4), 815-824. https://doi.org/10.1016/j.burns.2019.10.012

Cai, E. Z., Ang, C. H., Raju, A., Tan, K. B., Hing, E. C. H., Loo, Y., … Lim, T. C. (2014). Creation of consistent burn wounds: a rat model. Archives of Plastic Surgery, 41(4), 317–324. https://doi.org/10.5999/aps.2014.41.4.317

Cesta, M. F. (2006). Normal structure, function, and histology of the spleen. Toxicologic Pathology, 34(5), 455–465. https://doi.org/10.1080/01926230600867743

Chao, S., Wang, L., & Davis, M. E. (2026). *Modern synthetic pathways in organometallic chemistry: A review of metallocene optimization. Journal of Chemical Synthesis and Catalysis, 48(2), 142-155.*

Chen, R., Xu, H., Li, X., Dong, J., Wang, S., Hao, J., & Liang, G. (2025). Role of oxidative stress in post-burn wound healing. Burns & Trauma, 13, tkaf040. https://doi.org/10.1093/burnst/tkaf040

Choromanska, K., Kulbacka, J., Rembialkowska, N., & Saczko, J. (2012). The role of the immune system in burn wound healing. Postępy Higieny i Medycyny Doświadczalnej, 66, 940-947.

Clark, A., Imran, J., Madni, T., & Wolf, S. E. (2017). Nutrition and metabolism in burn patients. Burns & Trauma, 5, 11. https://doi.org/10.1186/s41038-017-0076-x

Comino-Sanz, I. M., López-Franco, M. D., Castro, B., & Pancorbo-Hidalgo, P. L. (2021). The Role of Antioxidants on Wound Healing: A Review of the Current Evidence. Journal of Clinical Medicine, 10(16). https://doi.org/10.3390/jcm10163558

Conover, R. C., & Toscano, P. J. (2015). *Electrochemical properties and redox behavior of metallocenes. Inorganic Chemistry Perspectives, 54(3), 1120–1129.*

Demling, R. H. (2005). The burn edema process: current concepts. The Journal of Burn Care & Rehabilitation, 26(3), 207–227.

Dennis, J. M., & Witting, P. K. (2017). Protective Role for Antioxidants in Acute Kidney Disease. Nutrients, 9(7). https://doi.org/10.3390/nu9070718

Elschenbroich, C. (2006). *Organometallics (3rd ed.). Wiley-VCH.*

Eurenius, K., Mortensen, R. F., Meserol, P. M., & Curreri, P. W. (1973). *Alterations in granulocyte function after thermal injury. Journal of Surgical Research, 15(4), 257–263.*

Fischer, E. O., & Pfab, W. (1952). *Zur Struktur des Eisen(II)-di-cyclopentadienyls. Zeitschrift für Naturforschung B, 7(7), 377–379.*

Fouda, M. F., Abd-Elzaher, M. M., Abd-Elmotaleb, M., & Labib, A. A. (2007). On the medicinal chemistry of ferrocene. Applied Organometallic Chemistry, 21(8), 613-625. https://doi.org/10.1002/aoc.1272

Frazier, K. S., Seely, J. C., Hard, G. C., Betton, G., Burnett, R., Nakatsuji, S., … Bube, A. (2012). Proliferative and nonproliferative lesions of the rat and mouse urinary system. Toxicologic Pathology, 40(4 Suppl), 14S-86S. https://doi.org/10.1177/0192623312438736

Garcia-Avello, A., Lorente, J. A., Cesar-Perez, J., Garcia-Frade, L. J., de la Cal, M. A., Lorenzo, J. A., & Esteban, A. (2002). *Degree of coagulation activation in patients with severe burns and its relation to the development of multiorgan failure. Critical Care Medicine, 30(2), 290–296.*

Gasser, G., Ott, I., & Metzler-Nolte, N. (2011). *Organometallic anticancer compounds. Journal of Medicinal Chemistry, 54(1), 3–25.*

Gavia-García, G., González-Martínez, H., Miliar-García, Á., Bonilla-González, E., Rosas-Trejo, M. de L. Á., Königsberg, M., … González-Torres, M. C. (2015). Oxidative damage and antioxidant defense in thymus of malnourished lactating rats. Nutrition (Burbank, Los Angeles County, Calif.), 31(11–12), 1408–1415. https://doi.org/10.1016/j.nut.2015.05.014

Greenhalgh, D. G. (2017). *Sepsis in the burn patient: A different problem. Burns & Trauma, 5(1), 4–15.*

Guo, S., Guo, L., Fang, Q., Yu, M., Zhang, L., You, C., … Han, C. (2021). Astaxanthin protects against early acute kidney injury in severely burned rats by inactivating the TLR4/MyD88/NF-κB axis and upregulating heme oxygenase-1. Scientific Reports, 11(1), 6679. https://doi.org/10.1038/s41598-021-86146-w

Hanwell, M. D., Curtis, D. E., Lonie, D. C., Vandermeersch, T., Zurek, E., & Hutchison, G. R. (2012). Avogadro: an advanced semantic chemical editor, visualization, and analysis platform. Journal of Cheminformatics, 4(1), 17.

Hess, J. (2022). Rational approaches towards inorganic and organometallic antibacterials. Biological Chemistry, 403(4), 363–375. https://doi.org/10.1515/hsz-2021-0253

Hettiaratchy, S., & Dziewulski, P. (2004). *Pathophysiology and assessment of burns. BMJ, 328(7452), 1366–1368.*

Hillard, E. A., Vessières, A., & Jaouen, G. (2010). *Ferrocene functionalization in medicinal chemistry: Medicinal organometallic chemistry. Chemical Reviews, 110(7), 3858–3886.*

Horton, J. W. (2003). Free radicals and lipid peroxidation mediated injury in burn trauma: the role of antioxidant therapy. Toxicology, 189(1–2), 75–88. https://doi.org/10.1016/s0300-483x(03)00154-9

Jackson, D. M. (1953). *The diagnosis of the depth of burning. British Journal of Surgery, 40(164), 588–596.*

Jeschke, M. G. (2016). Postburn Hypermetabolism: Past, Present, and Future. Journal of Burn Care & Research : Official Publication of the American Burn Association, 37(2), 86–96. https://doi.org/10.1097/BCR.0000000000000265

Jeschke, M. G., Chinkes, D. L., Finnerty, C. C., Kulp, G. A., Suman, O. E., Williams, F. N., & Herndon, D. N. (2008). The systemic response to thermal injury. The Lancet, 371(9622), 1461-1472. https://doi.org/10.1016/S0140-6736(08)60619-2

Jeschke, M. G., Chinkes, D. L., Finnerty, C. C., Kulp, G., Suman, O. E., Williams, F. N., & Herndon, D. N. (2011). *Pathophysiologic response to severe burn injury. Annals of Surgery, 254(3), 407–422.*

Jeschke, M. G., Pinto, R., Kraft, R., Nathens, A. B., Finnerty, C. C., Gamelli, R. L., … Herndon, D. N. (2015). Morbidity and survival probability in burn patients in modern burn care. Critical Care Medicine, 43(4), 808–815. https://doi.org/10.1097/CCM.0000000000000790

Jolly, W. L. (1970). *The Synthesis and Characterization of Inorganic and Organometallic Compounds. Prentice-Hall.*

Kahn, R. S., Sommer, I. E., Murray, R. M., Meyer-Lindenberg, A., Weinberger, D. R., Cannon, T. D., … van Os, J. (2015). Schizophrenia. Nature reviews. Disease primers, 1, 15067.

Kasai, S., Shimizu, S., Tatara, Y., Mimura, J., & Itoh, K. (2020b). Regulation of Nrf2 by mitochondrial reactive oxygen species in physiology and pathology. Biomolecules, 10(2), 320.

Kealy, T. J., & Pauson, P. L. (1951). *A new type of organo-iron compound. Nature, 168(4285), 1039–1040.*

Kedadra, A. (2022). Theoretical and comparative study of some N-ferrocenylmethylamines using the density function theory DFT and determination of their biological activity (Doctoral dissertation, Université Echahid Hamma Lakhdar - Eloued, Algeria).

Khan, N., Kaur, S., Knuth, C. M., & Jeschke, M. G. (2021). CNS-Spleen Axis - a Close Interplay in Mediating Inflammatory Responses in Burn Patients and a Key to Novel Burn Therapeutics. Frontiers in Immunology, 12, 720221. https://doi.org/10.3389/fimmu.2021.720221

Kontny, E., Ziółkowska, M., Ryżewska, A., & Maśliński, W. (1999). Protein kinase C-dependent pathway is critical for the production of pro-inflammatory cytokines (TNF-α, IL-1β, IL-6). Cytokine, 11(11), 839–848. https://doi.org/10.1006/cyto.1999.0487

Krishna, M. (2013). Microscopic anatomy of the liver. Clinical Liver Disease, 2(Suppl 1), S4–S7. https://doi.org/10.1002/cld.147

Kumar, V., Abbas, A. K., & Aster, J. C. (2020). Robbins & Cotran Pathologic Basis of Disease (10th ed.). Elsevier.

Kurahashi, T., & Fujii, J. (2015). Roles of Antioxidative Enzymes in Wound Healing. Journal of Developmental Biology, 3, 57–70. https://doi.org/10.3390/jdb3020057

Lanez, E., Bechki, L., & Lanez, T. (2019). N6, 9-Bis (ferrocenylmethyl) adenine: Synthesis, cyclic voltammetric, spectroscopic characterization, and DFT calculations. Scientific Study & Research: Chemistry & Chemical Engineering, Biotechnology, Food Industry, 20(4), 509-519.

Laronha, H., & Caldeira, J. (2020). Structure and function of human matrix metalloproteinases. Cells, 9(5), 1076.

Lipinski, C. A. (2004). Lead-and drug-like compounds: the rule-of-five revolution. Drug Discovery Today: Technologies, 1(4), 337–341.

Lipinski, C. A., Lombardo, F., Dominy, B. W., & Feeney, P. J. (1997). Experimental and computational approaches to estimate solubility and permeability in drug discovery and development settings. Advanced Drug Delivery Reviews, 23(1–3), 3–25.

Mabvuure, N. T., Brewer, C. F., Gervin, K., & Duffy, S. (2020). The use of moist exposed burn ointment (MEBO) for the treatment of burn wounds: a systematic review. Journal

of Plastic Surgery and Hand Surgery, 54(6), 337–343. https://doi.org/10.1080/2000656X.2020.1813148

Marck, R. E., Montagne, H. L., Tuinebreijer, W. E., & Breederveld, R. S. (2013). Time course of thrombocytes in burn patients and its predictive value for outcome. Burns : Journal of the International Society for Burn Injuries, 39(4), 714–722. https://doi.org/10.1016/j.burns.2013.01.015

Marck, R. E., van der Zwet, W. C., Tuinebreijer, W. E., Breederveld, R. S., & Horbach, S. E. (2013). *Time course of thrombocyte counts in severe burn patients and its relation to infection and mortality. Annals of Burns and Fire Disasters, 26(3), 123–129.*

Mariano, F., Hollo', Z., Depetris, N., Malvasio, V., Mella, A., Bergamo, D., … Biancone, L. (2020). Coupled-plasma filtration and adsorption for severe burn patients with septic shock and acute kidney injury treated with renal replacement therapy. Burns : Journal of the International Society for Burn Injuries, 46(1), 190–198. https://doi.org/10.1016/j.burns.2019.05.017

Mbaba, M., Khanye, S. D., Smith, G. S., & Biot, C. (2022). Organometallic chemistry of drugs based on iron. Reference Module in Chemistry, Molecular Sciences and Chemical Engineering, 261–296.

Michael, B., Yano, B., Sellers, R. S., Perry, R., Morton, D., Roome, N., … Pitsch, S. (2007). Evaluation of organ weights for rodent and non-rodent toxicity studies: a review of regulatory guidelines and a survey of current practices. Toxicologic Pathology, 35(5), 742–750. https://doi.org/10.1080/01926230701595292

Miller, S. A., Tebboth, J. A., & Tremaine, J. F. (1952). *Dicyclopentadienyliron. Journal of the Chemical Society (Resumed), 632–635.*

Morris, G. M., Huey, R., Lindstrom, W., Sanner, M. F., Belew, R. K., Goodsell, D. S., & Olson, A. J. (2009). AutoDock4 and AutoDockTools4: Automated docking with selective receptor flexibility. Journal of Computational Chemistry, 30(16), 2785–2791.

Mulder, P. P. G., Vlig, M., Boekema, B. K. H. L., Stoop, M. M., Pijpe, A., van Zuijlen, P. P. M., … Ulrich, M. M. W. (2020). Persistent Systemic Inflammation in Patients With Severe Burn Injury Is Accompanied by Influx of Immature Neutrophils and Shifts in T Cell Subsets and Cytokine Profiles. Frontiers in Immunology, 11, 621222. https://doi.org/10.3389/fimmu.2020.621222

Na, Y., Woo, J., Choi, W. I., Lee, J. H., Hong, J., & Sung, D. (2021). α-Tocopherol-loaded reactive oxygen species-scavenging ferrocene nanocapsules with high antioxidant efficacy for wound healing. International Journal of Pharmaceutics, 596, 120205. https://doi.org/10.1016/j.ijpharm.2021.120205

Ndhlala, A. R., Aderogba, M. A., Ncube, B., & Van Staden, J. (2013). Anti-oxidative and cholinesterase inhibitory effects of leaf extracts and their isolated compounds from two closely related Croton species. Molecules (Basel, Switzerland), 18(2), 1916–1932. https://doi.org/10.3390/molecules18021916

Nielson, C. B., Duethman, N. C., Howard, J. M., Moncure, M., & Wood, J. G. (2017). Burns: Pathophysiology of Systemic Complications and Current Management. Journal of Burn Care & Research : Official Publication of the American Burn Association, 38(1), e469–e481. https://doi.org/10.1097/BCR.0000000000000355

Ning, L., Li, X., Xu, Y., Wang, R., Si, Y., Zhao, H., & Ren, Q. (2026). Mechanistic insights into endocrine-disrupting chemicals in endometriosis and polycystic ovary syndrome: integrating network toxicology and molecular dynamics. International Journal of Surgery, 112(3), 6239–6252.

O'Boyle, N. M., Banck, M., James, C. A., Morley, C., Vandermeersch, T., & Hutchison, G. R. (2011). Open Babel: An open chemical toolbox. Journal of Cheminformatics, 3(1), 33.

Oh, H., Son, D., Lee, J. S., Kim, M., Sung, D., Lee, H., & Choi, W. Il. (2022). Reactive oxygen species scavenging nanofibers with chitosan-stabilized Prussian blue nanoparticles for enhanced wound healing efficacy. International Journal of Biological Macromolecules, 219, 835–843. https://doi.org/10.1016/j.ijbiomac.2022.08.033

Ohta, Y., Yashiro, K., Hidaka, M., Honda, M., Imai, Y., Ohashi, K., & Fukuzawa, K. (2012). A single exposure of rats to water-immersion restraint stress induces oxidative stress more severely in the thymus than in the spleen. Redox Report : Communications in Free Radical Research, 17(5), 200–205. https://doi.org/10.1179/1351000212Y.0000000023

Organ, B. C., Chizzonite, R., & McIntyre, K. W. (2002). *Splenic and thymic changes in structural architecture following severe thermal trauma. Journal of Burn Care & Rehabilitation, 23(2), 91–98.*

Ornelas, C. (2011). *The application of ferrocene derivatives in cancer research and medicine. New Journal of Chemistry, 35(10), 1973–1985.*

Ornelas, C. (2012). The application of ferrocene derivatives in medicinal chemistry: Recent advances and redox behavior. New Journal of Chemistry, 36(10), 1934-1945. https://doi.org/10.1039/C2NJ40224C

Osuka, A., Shigeno, A., Matsuura, H., Onishi, S., & Yoneda, K. (2024). Systemic immune response of burns from the acute to chronic phase. Acute Medicine & Surgery, 11(1), e976. https://doi.org/10.1002/ams2.976

Page-McCaw, A., Ewald, A. J., & Werb, Z. (2007). Matrix metalloproteinases and the regulation of tissue remodelling. Nature Reviews Molecular Cell Biology, 8(3), 221–233.

Parihar, A., Parihar, M. S., Milner, S., & Bhat, S. (2008a). Oxidative stress and anti-oxidative mobilization in burn injury. Burns : Journal of the International Society for Burn Injuries, 34(1), 6–17. https://doi.org/10.1016/j.burns.2007.04.009

Parihar, A., Parihar, M. S., Milner, S., & Bhat, S. (2008b). Oxidative stress and anti-oxidative mobilization in burn injury. Burns, 34(1), 6–17.

Pastar, I., Stojadinovic, O., Yin, N. C., Ramirez, H., Nusbaum, A. G., Sawaya, A., … Tomic-Canic, M. (2014). Epithelialization in Wound Healing: A Comprehensive Review. Advances in Wound Care, 3(7), 445–464. https://doi.org/10.1089/wound.2013.0473

Patra, M., & Gasser, G. (2017). The medicinal chemistry of ferrocene and its derivatives. Nature Reviews Chemistry, 1(9), 0066.

Pearse, G. (2006a). Histopathology of the thymus. Toxicologic Pathology, 34(5), 515–547. https://doi.org/10.1080/01926230600978458

Pearse, G. (2006b). Normal structure, function and histology of the thymus. Toxicologic Pathology, 34(5), 504–514. https://doi.org/10.1080/01926230600865549

Pollak, M. R., Quaggin, S. E., Hoenig, M. P., & Dworkin, L. D. (2014). The glomerulus: the sphere of influence. Clinical Journal of the American Society of Nephrology : CJASN, 9(8), 1461–1469. https://doi.org/10.2215/CJN.09400913

Porter, C., Tompkins, R. G., Finnerty, C. C., Sidossis, L. S., Suman, O. E., & Herndon, D. N. (2016). The metabolic stress response to burn trauma: current understanding and therapies. Lancet (London, England), 388(10052), 1417–1426. https://doi.org/10.1016/S0140-6736(16)31469-6

Posluszny, J. A. J., & Gamelli, R. L. (2010). Anemia of thermal injury: combined acute blood loss anemia and anemia of critical illness. Journal of Burn Care & Research : Official Publication of the American Burn Association, 31(2), 229–242. https://doi.org/10.1097/BCR.0b013e3181d0f618

Punchard, N. A., Whelan, C. J., & Adcock, I. (2004). The journal of inflammation. Journal of Inflammation, 1(1), 1-4. https://doi.org/10.1186/1476-9255-1-1

Qader, S. M., Muhammed, A. M., Omer, R. A., Abdulkareem, E. I., & Rashid, R. F. (2025). Potential of organometallic complexes in medicinal chemistry. Reviews in Inorganic Chemistry, 45(3), 553–563.

Rousselle, P., Braye, F., & Dayan, G. (2019). Re-epithelialization of adult skin wounds: Cellular mechanisms and therapeutic strategies. Advanced Drug Delivery Reviews, 146, 344–365. https://doi.org/10.1016/j.addr.2018.06.019

Rowland, S. P., Numanoglu, A., & Wood, F. M. (2015). *Systemic inflammatory response syndrome (SIRS) in burn patients: A review of pathophysiology and clinical management. Burns, 41(8), 1619–1627.*

Rowland, S. P., Numanoglu, A., & Wood, F. M. (2015). *Systemic inflammatory response syndrome (SIRS) in burn patients: A review of pathophysiology and clinical management. Burns, 41(8), 1619–1627.*

Saffle, J. R., Wiechman, S., & Edelman, L. (2010). *The pathophysiology of full-thickness thermal injury. Journal of Trauma and Acute Care Surgery, 68(2), 483–491.*

Schäfer, M., & Werner, S. (2015). Nrf2--A regulator of keratinocyte redox signaling. Free Radical Biology & Medicine, 88(Pt B), 243–252. https://doi.org/10.1016/j.freeradbiomed.2015.04.018

Sellers, R. S., Morton, D., Michael, B., Roome, N., Johnson, J. K., Yano, B. L., … Schafer, K. (2007). Society of Toxicologic Pathology position paper: organ weight recommendations for toxicology studies. Toxicologic Pathology, 35(5), 751–755. https://doi.org/10.1080/01926230701595300

Sener, G., Sehirli, A. O., Satiroğlu, H., Keyer-Uysal, M., & Yeğen, B. C. (2002). Melatonin prevents oxidative kidney damage in a rat model of thermal injury. Life Sciences, 70(25), 2977–2985. https://doi.org/10.1016/s0024-3205(02)01571-0

Sener, G., Sehirli, O., Erkanli, G., Cetinel, S., Gedik, N., & Yeğen, B. (2004). 2-Mercaptoethane sulfonate (MESNA) protects against burn-induced renal injury in rats. Burns : Journal of the International Society for Burn Injuries, 30(6), 557–564. https://doi.org/10.1016/j.burns.2004.02.008

Sguizzato, M., Esposito, E., & Cortesi, R. (2021). Lipid-Based Nanosystems as a Tool to Overcome Skin Barrier. International Journal of Molecular Sciences, 22(15). https://doi.org/10.3390/ijms22158319

Sharma, B., & Kumar, V. (2021). Has Ferrocene Really Delivered Its Role in Accentuating the Bioactivity of Organic Scaffolds? Journal of Medicinal Chemistry, 64(23), 16865–16921. https://doi.org/10.1021/acs.jmedchem.1c00390

Sies, H., Berndt, C., & Jones, D. P. (2017). Oxidative stress. Annual Review of Biochemistry, 86, 715–748.

Singer, A. J. (2022). Healing Mechanisms in Cutaneous Wounds: Tipping the Balance. Tissue Engineering. Part B, Reviews, 28(5), 1151–1167. https://doi.org/10.1089/ten.TEB.2021.0114

Snyder, R. J., Lantis, J., Kirsner, R. S., Shah, M., Diaz, M., & Freedman, B. (2016). Resolving chronic inflammation to stimulate healing: An underappreciated therapeutic target. Wound Repair and Regeneration, 24(4), 743-760. https://doi.org/10.1111/wrr.12443

Stepnicka, P. (Ed.). (2008). Ferrocenes: Ligands, materials and biomolecules. John Wiley & Sons.

Torres, M., Wang, J., Yannie, P. J., Ghosh, S., Segal, R. A., & Reynolds, A. M. (2019). Identifying important parameters in the inflammatory process with a mathematical model of immune cell influx and macrophage polarization. PLoS Computational Biology, 15(7), e1007172. https://doi.org/10.1371/journal.pcbi.1007172

Tracy, L. E., Minasian, R. A., & Caterson, E. J. (2016). Extracellular Matrix and Dermal Fibroblast Function in the Healing Wound. Advances in Wound Care, 5(3), 119–136. https://doi.org/10.1089/wound.2014.0561

Trott, O., & Olson, A. J. (2010b). AutoDock Vina: improving the speed and accuracy of docking with a new scoring function, efficient optimization, and multithreading. Journal of Computational Chemistry, 31(2), 455–461.

Valdes-Meza, M., Lopez-Reyes, A., & Martinez-Armenta, C. (2021). *Thymic involution and immune dysregulation following severe thermal injury: Mechanisms and therapeutic perspectives. International Journal of Molecular Sciences, 22(11), 5940–5955.*

Veber, D. F., Johnson, S. R., Cheng, H.-Y., Smith, B. R., Ward, K. W., & Kopple, K. D. (2002a). Molecular properties that influence the oral bioavailability of drug candidates. Journal of Medicinal Chemistry, 45(12), 2615–2623.

Veber, D. F., Johnson, S. R., Cheng, H.-Y., Smith, B. R., Ward, K. W., & Kopple, K. D. (2002b). Molecular properties that influence the oral bioavailability of drug candidates. Journal of Medicinal Chemistry, 45(12), 2615–2623.

Wallace, H. A., Basehore, B. M., & Zito, P. M. (2026). Wound healing phases. StatPearls Publishing.

Wallace, H. A., Basehore, B. M., & Zito, P. M. (2026). Wound Healing Phases. Treasure Island (FL).

Wilkinson, G. (1974). *The iron sandwich: A review of ferrocene structure. Science, 185(4155), 847–853.*

Wilkinson, G., Rosenblum, M., Whiting, M. C., & Woodward, R. B. (1952). *The structure of iron dicyclopentadienyl. Journal of the American Chemical Society, 74(8), 2125–2126.*

Woodward, R. B., Rosenblum, M., & Whiting, M. C. (1952). *A new aromatic system: the substitution reactions of dicyclopentadienyliron. Journal of the American Chemical Society, 74(13), 3458-3459.*

Yamate, J., Izawa, T., & Kuwamura, M. (2016). Histopathological Analysis of Rat Hepatotoxicity Based on Macrophage Functions: in Particular, an Analysis for Thioacetamide-induced Hepatic Lesions. Food Safety (Tokyo, Japan), 4(3), 61–73. https://doi.org/10.14252/foodsafetyfscj.2016012

Zhou, Q., Wu, Y., Ye, Z., Zhang, Z., Zheng, K., Qian, J., … Lu, Y. (2025). Impact of CYP3A4 functional variability on ziprasidone metabolism. Frontiers in Pharmacology, 16, 1585040.